STOCHASTIC GEOMETRY BASED ANALYSIS OF HETEROGENEOUS NETWORKS

by

Ceren Sevinç

B.S., Electrical and Electronics Engineering, Boğaziçi University, 2013

Submitted to the Institute for Graduate Studies in
Science and Engineering in partial fulfillment of
the requirements for the degree of
Master of Science

Graduate Program in Electrical and Electronics Engineering
Boğaziçi University
2016

ACKNOWLEDGEMENTS

I would like to express my most sincere gratitude to my advisor Mutlu Koca in the first place. We have all experienced turning points in our lives, although some of them have greater influence and impact than the others. Taking *Digital Communication* course from Prof. Koca was one of my biggest turning points. After completion of undergraduate education, I was standing in a situation in which I had to decide whether to continue working in a company or to pursue an academic career. His enthusiasm and support gave me courage to walk through this academic path. Without a doubt, this work would not have been present without his support and guidance.

I owe thanks to Prof. Hakan Deliç for all that I learned from him during my education. It was always a pleasure to follow the lectures that he taught. I am also grateful to my committee members, Prof. Emin Anarım and Assoc. Prof. Güneş Karabulut Kurt for their valuable comments and suggestions.

I am thankful to all of my friends in WCL and BUSIM for making this journey an unforgettable memory. I owe special thanks to Alican Gök for being not just a good colleague, but a true friend. Their friendship and support always remind me how lucky I am to be a part of Bogazici family.

Finally, I would like to thank my parents who always respect my decisions and choices and encourage me to do well throughout my entire life.

This work is supported by the Bogazici University Research Fund under Contract 9201.

ABSTRACT

STOCHASTIC GEOMETRY BASED ANALYSIS OF HETEROGENEOUS NETWORKS

Recent cellular systems are composed of multiple tiers of access points with dense base station deployments in order to maintain higher coverage region and network capacity. Classical methods of modeling base station deployments such as hexagonal grid or square grid modeling are mostly insufficient to analyze characteristics of the real geometric configuration. As a result, stochastic geometry approach has been suggested to provide analytically tractable models of ad hoc wireless networks. Since the interference is a primary limitation factor of the capacity of wireless networks and the quality of service, inter-cell interference coordination (ICIC) is suggested to enhance the performance of the network, especially in heterogeneous networks. We are mainly focused on the performance of the strict fractional frequency reuse (FFR) and soft frequency reuse (SFR) schemes, which are the two most commonly used ICIC techniques. Since small cells are becoming an essential part of future LTE networks, it is vital to investigate the impact of user mobility on heterogeneous networks. We examine different approaches for mobility evaluation of cellular networks by providing single snapshot analysis of the interference and coverage probability.

ÖZET

HETEROJEN AĞLARIN STOKASTİK GEOMETRİ TEMELLİ ANALİZİ

Yakın dönem hücresel sistemler, kapsama bölgesini ve ağ kapasitesini artırmak amacıyla yoğun baz istasyonu konuşlanmaları içeren çoklu katmanlı erişim noktalarından oluşmaktadır. Altıgen ya da kare ızgara gibi klasik baz istasyonu dağıtım modelleri, gerçek geometrik kurulumların özelliklerini analiz etmek için yetersizdir. Bu türden plansız telsiz ağların analitik olarak çözümlenebilmesi için stokastik geometri yaklaşımı,önerilmiştir. Girişim, kablosuz ağların kapasitesini etkileyen en önemli faktörlerden biri olduğu için, hücreler-arası girişim eşgüdümü (ICIC), özellikle heterojen ağlarda, ağın başarımını artırmak için önerilmektedir. Çalışmamız, en sık kullanılan iki ICIC yöntemi olan katı kesirli frekans yeniden kullanımı (FFR) ve yumuşak yeniden kullanım (SFR) üzerinde yoğunlaşmıştır. Küçük hücreler, gelecek dönem LTE ağlarının artık vazgeçilmez bir parçası haline geldiği için, heterojen ağlarda kullanıcı hareketliliğinin etkisini araştırmak büyük önem taşımaktadır. Bu bağlamda, girişimin ve kapsama olasılığının anlık görünümlerinin analizini sağlayan farklı hareketlilik değerlendirmesi yaklaşımları incelenmiştir.

TABLE OF CONTENTS

LIST OF FIGURES

LIST OF TABLES

LIST OF SYMBOLS

$B(x, r)$	Ball of a radius r centered at x
F_{FFR}	CCDF of the edge user
g	Channel gain
I_r	Interference
I_{edge}	Interference caused by the cell-edge users
I_{int}	Interference caused by the interior users
k	Type of the tier
$\mathcal{L}$	Laplace functional
M	Total number of nodes
P	Transmit power
p_c	Coverage probability
P_{edge}	Transmit power of the base station for an edge user
P_{int}	Transmit power of the base station for an interior user
$P_x^!$	Reduced Palm distribution
R_z	Distance between interfering base stations and the user
$\mathbb{R}^d$	d-dimensional Euclidean space
T	SINR threshold
T_{FR}	Frequency reuse threshold
y	User index
$\mathbb{Z}$	Set of interfering base stations
α	Path loss exponent
β	Power control factor
δ	Allocated sub-band
Δ	Reuse factor
Δt	Time duration
λ	Intensity measure or density
μ	Mean value

Φ	Point process on $\mathbb{R}^d$
σ^2	Noise power
θ	Random angle
$\bar{v}$	Average velocity

LIST OF ACRONYMS/ABBREVIATIONS

1G	1st generation
2G	2nd generation
3G	3rd generation
3GPP	3rd generation partnership project
4G	4th generation
AP	Access point
BS	Base station
CCDF	Complementary cumulative distribution function
CDMA	Code division multiple access
eNB or eNodeB	Evolved node B
FAP	Femtocell access points
FDD	Frequency division duplex
FFR	Fractional frequency reuse
GSM	Global system for mobile communications
HCN or HetNet	Heterogeneous cellular networks
HeNB	Home evolved node B
ICI	Inter-cell interference
ICIC	Inter-cell interference coordination
LTE	Long term evolution
LTE-A	Long term evolution-advanced
MANET	Mobile ad hoc networks
MBS	Macro base station
MIMO	Multiple input multiple output
OFDM	Orthogonal frequency division multiplexing
OFDMA	Orthogonal frequency division multiple access
PCP	Poisson cluster process
PGFL	Power generating functional
PLP	Poisson line process

PPP	Poisson point process
QoS	Quality of service
RMM	Radio resource management
RWP	Random way point
SC-FDMA	Single carrier frequency division multiple access
SFR	Soft frequency reuse
SINR	Signal to interference plus noise ratio
TDD	Time division duplex
UMTS	Universal mobile telecommunications system
WCDMA	Wideband code division multiple access

1. INTRODUCTION

1.1. The 3rd Generation Partnership Project (3GPP)

3GPP was found in December 1998 to determine technical specifications and reports for a third generation (3G) mobile system which is based on evolved global system for mobile communication (GSM) networks and the radio access technologies (RAT) which support two main types of full duplexing modes: time division duplex (TDD) and frequency division duplex (FDD).

3GPP unites seven standard development organizational partners from Asia, North Ameriaca and Europe, which are ARIB, ATIS, CCSA, ETSI, TSDSI, TTA, TTC and provides a stable communication environment to generate the reports and complete specifications which determines 3GPP technologies such as cellular communications network technologies containing the core transport network, radio access, and service capabilities. These specifications cover developments on codecs, security, quality of service.

3GPP has four technical specification groups (TSG), which are Core Network and Terminals (CT), GSM EDGE Radio Access Networks (GERAN), Radio Access Networks (RAN) and Service and Systems Aspects (SA) . The 3GPP technologies from these groups are steadily evolving through next generations of commercial cellular telecommunications systems. 3GPP has come into the focus for cellular mobile network systems beyond 3G with the fulfillment of the first LTE specifications.

The main target for all 3GPP releases is to accomplish the system forwards and backwards compatible to guarantee that the operations will not be interrupted. As a recent example of this principle, backward compatibility between long term evolution (LTE) and LTE-Advanced (LTE-A) is one of the primary focal point of 3GPP in order that an LTE-A terminal works compatibly in an LTE mobile network, while an LTE terminal can work compatibly in the LTE-A mobile network.

1.2. Long Term Evolution (LTE)

In 2008, 3GPP project has introduced LTE as an extension of both universal mobile telecommunications system (UMTS) and code division multiple access (CDMA) in release 8 for the very first time. LTE provides up to 50 times performance improvement and much better spectral efficiency by supporting flexible bandwidth management compared to previous cellular systems.

Historical development stages in cellular technology reveals how much improvement is provided by the evolution of LTE. In early 1980's, first generation (1G) mobile system whose technology has been based on analog cellular technologies was used for only voice calls. In 1992, second generation (2G) with a digital technology has provided data throughput up to 14.4 kbps for voice communication and messaging. In 1998, 3GPP introduced 3G mobile system with regard to meet the increasing demand for data traffic. In 3G, both high speed packet switching capability and circuit switched voice transmission have been provided. Underlying technology is based on wideband code division multiple access (WCDMA), which has 2 Mbps peak data rate in downlink and 1 Mbps in the uplink, high speed packet access (HSPA) and its enhancements HSPA Plus (HSPA+). This infrastructure enables the developments of smart phone technologies such as web browsing, sending and receiving emails and video downloading in cellular devices.

The demand for higher data rate has increased extremely with the widespread use of always-on devices such as smart phones and tablets. Hence finding a new radio access technology (RAT) with a new network architecture has become inevitable. LTE does not require a dedicated line to make a call, since LTE uses a packet-switched network technology to transmit data and provide voice services, whereas previous mobile telephone systems uses a circuit-switched network.

LTE can accommodate both frequency division duplex (FDD) and time division duplex (TDD) mode and allows flexible carrier bandwidth ranging from 1.4 MHz to 20 MHz in addition to FDD and TDD. All LTE devices are required to support multiple

input multiple output (MIMO) transmissions, allowing trasmitting BS to send the data streams over the same carrier at the same time. LTE employes orthogonal frequency division multiple access (OFDMA), which is the extension of OFDM, with a peak transmission rate of 100 Mbps in 20 MHz channel for downlink transmission and single carrier frequency division multiple access (SC-FDMA) with a peak rate of 50 Mbps in 20 MHz channel for uplink transmission [5].

In 2010, complete integration of LTE femtocells are introduced in the form of the Home eNodeB (HeNB) in release 9 [6].

1.3. Femtocells

Femtocells might be considered as small, low-power base stations, which connect to the network of the mobile service provider via cable broadband connections or DSL. Figure 1.1 depicts the typical scenario which is composed of macrocell and femtocells.

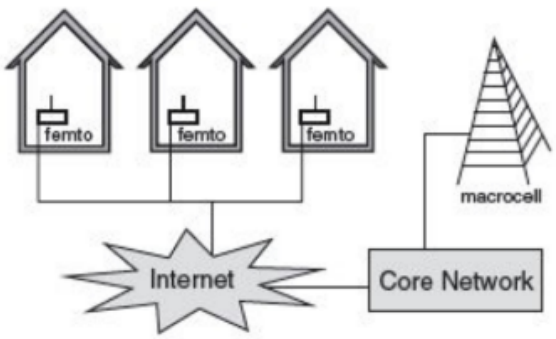

Figure 1.1. Femtocell and macrocell example [1].

As a result of Shannon's law, which makes a connection between the capacity (in bits/second) and SINR, femtocells provide a good potential to improve capacity. Most widely used pathloss model in the calculation of SINR is $Ad^{-\alpha}$, where A is a constant loss factor, d is the distance between the receiver and transmitter, and α is the path-loss exponent. Hence, it can be concluded that minimizing d is one of the key opportunity to increase the capacity. Besides, interference from neighboring cells will be mitigated and battery life will be prolonged, since femtocells have lower transmit power. Apart from these, frequency reuse schemes, diversity and interference cancellation techniques

can be employed as well to bolster the network capacity. More mobile users who are assigned to the same subbands of the spectrum can be served in a given area thanks to reduced interference and it leads to increase in the the area spectral efficiency or, in other words, the total number of active mobile users per Hz per unit area [7].

The other advantages of femtocells are listed in [8] as follows:

- They provide an improved macrocell reliability, since the indoor traffic can be offloaded to femtocell network over the IP backbone, resulting in better reception for mobile user that are connected to the macrocell BS.
- They decrease the operating and capital expenditure costs for operators, since femtocell deployment is less costly compared to adding macro BSs.
- They reduce the subscriber turnover by improving the coverage and capacity, hence, increasing the customer satisfaction.

1.4. Access Technologies

Most commonly used spectrum access policies for femtocells are open access and closed access. In open-access strategy, all mobile users (subscribers and non-subscribers) have a right to take a service from femtocells if they pass nearby. Conversely, in closed-access strategy, only subscribed cellular users that are licensed are allowed to be served by femtocells.

Closed access strategy provides more privacy and security for subscribed users, while open access strategy enhances the overall capacity and coverage of the network. Due to these tradeoffs, hybrid solutions are considered by reserving certain amount of femtocell resources to registered users only and allocating other resources for roamers.

In open access policy, handoffs from the macrocell to the femtocell can be cumbersome since there are large number of femtocells within the vicinity of macrocells. There might be channel fluctuations, as well, which causes a moving macrocell user to perform multiple handovers. Low complexity algorithms that take the presence of fem-

tocells into consideration should be applied in order to avoid unnecessary handovers by estimating the dwell time before handing off a macrocell user to an adjacent femtocell.

1.5. Wireless Ad Hoc Networks

When the network topology is known, service operator can set up the rules of fixed hierarchical structure of the transport layer. That being said, there is no centralized control which enables the hierarchical information flow in ad hoc networks. There are sets of mobile or static communication devices (i.e. nodes) in ad hoc networks. Ad hoc network topology can change constantly because of the mobility and nodes have to self-organize themselves since there is no centralized control. Especially in the 4th Generation (4G) and further generations, telecommunication systems will be in the form of heterogeneous networks which consists networks access devices, roaming mobile users, cars, computers even fridges and microwaves that will sense each other and self-organize their access to the network resources [9]. Randomness in the network structure itself makes the stochastic geometry tools necessary for analysis and development of the telecommunications networks.

1.6. ICIC Mitigation Techniques

Since subcarriers of intra-cell users are orthogonal to each other in orthogonal frequency division multiple access (OFDMA), the main source of interference comes from the inter-cell interference (ICI), particularly for the users at the cell edges . Inter-cell interference coordination (ICIC) strategies have been suggested to improve coverage probability and the throughput of users, while maximizing spatial reuse [10].

Widely used method for ICIC is fractional frequency reuse approach. In fractional frequency reuse method, each cell is split into two separate regions: cell-interior which accommodates interior users, and cell-edge which accommodates exterior users. The spectrum is subdivided into smaller parts in order that cell-edge users of adjacent cells do not interfere with each other. Besides, the interference for interior users diminishes.

The two most commonly used schemes of fractional frequency reuse (FFR) are strict FFR and soft frequency reuse (SFR).

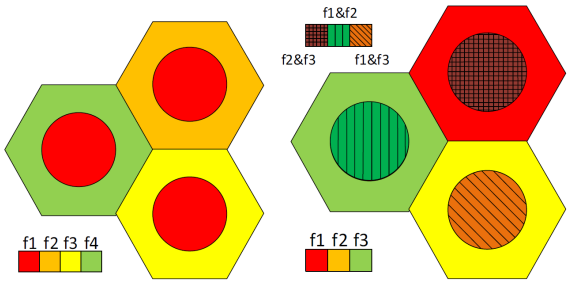

(a) Strict FFR (b) Soft FFR

Figure 1.2. Fractional frequency reuse schemes: Strict FFR and SFR [2].

In strict FFR, a shared subband of frequencies is assigned to the users in the cell centers, whereas the remaining spectrum is subdivided into different and mutually orthogonal frequency subbands, as illustrated in Figure 1.2 (a). Since users in the cell centers do not have a subband in common with cell-edge users, the interference is mitigated for both exterior and interior users.

In SFR, edge users of adjacent cells again use mutually orthogonal subbands, while the interior users of a specific cell is granted to share the cell-edge subbands of the adjacent cells. SFR provides improvement in coverage performance of exterior users by using power control factor. Although SFR is more efficient in terms of bandwidth utilization than strict FFR, it is disadvantageous in the sense of interference, hence coverage.

1.7. Related Work

In cellular network systems, more than 60% of calls and 90% of data services take place indoors [11]. Thus, it is crucial to have good indoor coverage for both voice and high speed data services. In the recent studies, one of the suggested methods to improve coverage is to use femtocell access points (FAPs) besides macrocell base stations (MBSs). Heterogeneous cellular networks (HCN or HetNet) which consist of overlaid deployment of macro, micro, pico, and femtocells, are expected to be used

widely in the future [12]. The biggest advantage of femtocell usage is a significant enhancement in the system spatial spectral efficiency [8].

Emerging needs entail large wireless systems with ad hoc networks and cellular networks. Classical methods of modeling base station deployments such as hexagonal grid or square grid modeling are mostly insufficient to analyze characteristics of the real geometric configuration. The coverage probability and capacity of the wireless networks can be obtained by using the properties and tools of stochastic geometry. Most used approach is to model location of the base stations in a random manner by using Poisson point process (PPP), whose use of PPP in networks date backs to 1997 [13], [14]. Since then extensive studies have been carried out to investigate the limits and performance characteristics of PPP deployment in ad hoc networks [15] [16] [17], and mobile ad-hoc networks (MANET) [18] [19].

A widely accepted model for BS deployment in wireless network is the homogeneous PPP and it is a favorable approach for several reasons. Firstly, it is tractable and easy to handle to fit a model for large-scale ad-hoc networks with random multiple access methods. Secondly, it provides tight bounds for the performance metrics in planned infrastructure-based networking systems and coordinated spectrum access networks [20]. In [21], [22], it is shown that PPP model provides more accurate approximation of an actual base station deployment than grid model.

In 2000, authors in [15] laid out that interference is a major limitation source of the capacity of wireless networks and the quality of service (QoS). Since signals from intra-cell users of OFDMA network are orthogonal to each other, the main interference is caused by inter-cell interference. Therefore, inter-cell interference coordination (ICIC) methods are suggested to enhance the performance of the network. ICIC strategies, especially in heterogeneous networks, become crucial to ensure certain level of QoS, since the tiers have overlapping sources. Authors in [23], [3] provide a detailed approach on the analysis of coverage and capacity under ICIC strategies for single tier network and HetNets respectively.

In order to take the advantage of diversity gain to increase the network coverage, authors in [24] provide the coverage probability expression which considers both ICIC and intra-cell diversity (ICD) in the case where there is temporal or spectral correlation between the interference and signal.

As stated previously, femtocells are a solution that helps to improve the coverage and capacity of the system. However, after adding small cells to the existing macrocell network, the avoidance of interference becomes a critical issue to be handled. Type of access control policy, which decides access permits of users to the femtocell, should be chosen wisely to limit the interference while enhancing the spectral efficiency. There are three main spectrum access policies for femtocells in a HCN: the open-access, closed-access and hybrid access policies. One may refer to [25] for a detailed survey on access models. Authors in [26] provides analytically tractable results by modeling femtocell and cellular user positions with a spatial random process under different access policies. Apart from the problem of interference and access policies, deployment of small cells in a pre-deployed network structure is also another issue that needs to be addressed. Presented study in [27] uses a novel dynamic network architecture model which is based on game theory and stochastic geometry in order to solve the problem of when and where to deploy small cells to take the advantage of high peak transmission rates, high energy efficiency and high spectral efficiency of small cells. They also provide a model which solves the joint problem of user resource sharing and operator pricing as a non-cooperative game.

Arshad et al. in [28] introduce an analytical method by employing stochastic geometry in order to determine the effect of handover delay on the average user rate in single-tier highly dense 5G cellular networks. Authors in [29] have investigated the impact of user mobility based on stochastic geometry by including the effect of handoff rate while determining the coverage probability in multi-tier networks. The stochastic characteristics of random walk and random way point (RWP) mobility models are examined in [30] and [31]- [32], respectively. [33] provides an analytical study of RWP mobility model and its impact on handover rate and sojourn time, which are two important cellular network parameters, for both PPP and deterministic hexagonal BS

models.

Another approach to mobility is to consider the fluctuations of the channel gains which are introduced by node mobility as another type of fading in additions to multi-path effects. Under this approach, the outage probability is derived in [34]. They also showed that distribution of the interference remains the same under high mobility and random walk models, while it increases under RWP mobility model.

Although modeling the BS nodes with a homogeneous (or stationary) PPP is the analytically advantageous and widely accepted presumption, the distribution of BS nodes can not be completely spatially random in each case and might be clustered. Authors in [35] suggest a numerically integrable formula for the outage probability and closed-form upper and lower bounds under Neyman-Scott cluster process model. Moreover, user locations can be dependent of the BS locations, in other saying, the BSs are deployed at densely populated regions. This correlation can be modeled by using a Poisson cluster process (PCP) model in which the femtocells are assumed to be placed at the cluster center as in [36]. Besides, femtocell deployments may exhibit clustered distribution and they can also be modeled by using PCP as in [37].

As a particular case of a Poisson field with a dense clustering, Poisson-line field of interfering nodes are used in modeling in [4]. This model suggests a reasonable model for the cases in which vehicles are distributed on a straight road at random. They have provided numerically tractable expressions for the speed of packet progression and end-to-end delay metrics for Poisson line process (PLP). Analytical formulas for the uplink coverage probability for a Poisson line tessellation have been derived in [38] by performing several shot-noise computations.

Our study assumes Rayleigh fading to obtain closed-form expressions. Apart from Rayleigh fading, if Gamma distribution (e.g., Nakagami-m) is selected as the channel power gain, the coverage probability can be formulated by the higher-order derivative of the Laplace transform of interference. [39] gives expressions of interference functionals and coverage probability in a Poisson network for Nakagami fading caused by multipath

propagation.

By taking power control into account, coverage probability of uplink under stochastic geometry has been provided in [40]. Multi-antenna HetNets have been studied in [41, 42]. Authors in [43] propose a unified stochastic-geometry based analytical method to evaluate not only outage probability and ergodic rate, but also error probability for cellular networks with different MIMO configurations. [44] presents tractable framework for outage probability and average ergodic rate in downlink HCNs with flexible cell association policies by using bias factor.

In [45], it is shown that SIR distributions of different cellular network models can be approximately found by a certain horizontal shift of the distribution of PPP model by considering mean interference-to-signal ratio between the network model and PPP model. Wei et al. in [46] propose a generalization of this approach to HetNets and use approximation approaches to calculate distribution of the SIR based on PPP and mean interference-to-signal ratio based gain for each individual tier of HetNets and show that their approximate results provide a good approximation compared to derived exact distribution of the SIR in two-tier HetNets modeled by Ginibre and PPP.

Intensity matching approach by using stochastic geometry perspective is introduced in [47] so as to estimate the effects of propagation and blockage models on key system parameters such as density of BSs, besides area spectral efficiency and throughput are computed by using the outlined approach.

1.8. Organization

The rest of the thesis is organized as follows: In Chapter 2, we present the tools of stochastic geometry that will be used in other chapters. In Chapters 3 and 4, we provide performance evaluation of single tier and multi-tier networks, respectively, under strict FFR and SFR schemes. In Chapter 5, mobility evaluation of cellular networks are investigated by providing different approaches to handling mobility. The thesis is concluded in Chapter 6.

2. STOCHASTIC GEOMETRY OVERVIEW

One of the key performance metrics of the networks is signal to inference plus noise ratio (SINR), which is characterized by the ratio of received signal power to the total received from all interferers, plus the thermal noise power at the receiver. Based on SINR, bit error rate in the link between the transmitter and the user will be affected; hence this will determine whether the user will be covered and what will be the maximum achievable data rate if the user is covered. Therefore, the spatial distribution of the SINR needs to be known in order to optimize the HetNets.

The performance of the modern cellular systems depends strongly on the locations of the base stations or users, which need to be modeled as a stochastic process of points due to the intrinsic uncertainty of the model itself. Hence, stochastic geometry, particularly point process theory, is a very convenient tool for modeling and analyzing wireless networks. Since PPP has the complete spatial randomness or independence property, it provides tools which are easy to analyze [48].

Stochastic geometry based calculation of SINR distribution in HetNets provides analytically tractable models and scalable results to an arbitrary number of tiers. Assuming the locations of BSs in the tiers are distributed according to PPP, distribution of the SINR at an arbitrary location in the network can be calculated exactly and depends only on certain network deployment parameters [49].

PPP has a central position among other process models for several reasons as outlined in [50]. Firstly, PPP model can be considered as a null-model to make a basis for comparison of completely random processes with other point-patterns such as cluster point processes. Secondly, PPP model is useful for simulation procedures. For instance, PPP model needs to be constructed first and modified accordingly in order to simulate Poisson germ-grain model or Neyman-Scott processes.

2.1. Poisson Point Process

Consider a spatial point process (p.p.) Φ which is a random and finite collection of points in the d-dimensional Euclidean space $\mathbb{R}^d$. Any given realization Φ of a p.p. can be viewed as a discrete subset $\Phi = \{x_i\} \subset \mathbb{R}^d$ of the space.

Alternatively, Φ can be regarded as a point measure or counting measure $\Phi = \sum_i \epsilon_{x_i}$, where ϵ_x is the Dirac measure at x; for $A \subset \mathbb{R}^d$, $\epsilon_x(A) = 1$ if $x \in A$ and $\epsilon x(A) = 0$ if $x \notin A$. Consequently, $\Phi(A)$ indicates the number of points of p.p. Φ in A. Besides, $\sum_i f(x_i) = \int_{\mathbb{R}^d} f(x)\Phi(dx)$ is valid for all real functions f which are defined on $\mathbb{R}^d$.

The distribution of a p.p. is completely described by the family of finite dimensional distributions $(\Phi(A_1), ..., \Phi(A_k))$, where $A_1, ..., A_k$ run over the bounded subsets of $\mathbb{R}^d$ as in the case of other stochastic processes.

Outlined definitions and theorems that are related to point processes in here will be prominent tools to analyse the key performance metrics of SINR distributions in the next chapters.

Definition 2.1.1. Poisson Point Process (PPP)

For Λ which represents a locally finite measure on $\mathbb{R}^d$, the PPP Φ of density measure λ can be defined with the help of its finite-dimensional distributions as in [51] such that

$$\mathbf{P}\left\{\Phi(A_1) = n_1, ..., \Phi(A_k) = n_k\right\} = \sum_{i=1}^{k} \left(e^{\Lambda(A_i)} \frac{\Lambda(A_i)^{n_i}}{n_i!}\right)$$

for every $k = 1, 2, ...$ and all bounded, mutually disjoint sets A_i for $i = 1, ..., k$. If $\Lambda(dx) = \lambda dx$ is a multiple of Lebesgue measure in $\mathbb{R}^d$, then Φ is called a homogeneous PPP and λ is its intensity or density parameter.

Definition 2.1.2. Probability generating functional (PGFL)

Let $f : \mathbb{R}^d \to \mathbb{R}^+$, then PGFL of a homogeneous PPP is defined as

$$\mathcal{P}_\Phi(f) = \mathbb{E}\left[\sum_{x\in\Phi} f(x)\right] = exp\left(-\lambda \int_{\mathbb{R}^d} (1 - f(x))dx\right).$$

The PGFL is a useful tool for converting an expectation of a product of the points, hence the sum of the exponents, in the PPP into an integral.

Definition 2.1.3. Laplace Functional

The Laplace functional $\mathcal{L}$ of a point process Φ is defined as

$$\mathcal{L}_\Phi(f) = \mathbf{E}\left[exp(-\textstyle\int_{\mathbb{R}^d} f(x)\Phi(dx)\right]$$

where f is defined on the set of all non-negative functions on $\mathbb{R}^d$.

Unlike PGFL, which is mostly restricted to random counting measures, the Laplace functional is defined for general non-negative random measures. The Laplace functional does not depend on the random measure itself, but only on its distribution.

Definition 2.1.4. Laplace Functional of PPP

The Laplace functional of the PPP of intensity measure Λ is calculated by

$$\mathcal{L}_\Phi(f) = exp\left(-\textstyle\int_{\mathbb{R}^d}(1 - e^{-f(x)})\Lambda(dx)\right).$$

Definition 2.1.5. Campbell's theorem

Let Φ be a p.p. on $\mathbb{R}^d$ with an intensity function λ and $f : \mathbb{R}^d \mapsto \mathbb{R}$ be a measurable function. Then the random sum

$$S = \sum_{x \in \Phi} f(x)$$

is a random variable with mean

$$\mathbb{E}[S] = \mathbb{E}\left[\sum_{x \in \Phi} f(x)\right] = \int_{\mathbb{R}^d} \lambda(x) f(x) dx.$$

If $\Phi \subset \mathbb{R}^d$ is a stationary p.p. with intensity λ, then the mean of the sum $S = \sum_{x \in \Phi} f(x)$ becomes

$$\mathbb{E}[S] = \lambda \int_{\mathbb{R}^d} f(x) dx.$$

Significance of Campbell's theorem becomes apparent in the evaluation of the functional expectations of a PPP, which requires conversion of a sum into an integral. Laplace transform of a PPP can be computed by combining the outcomes of PGFL and Campbell's theorem as follows

$$\mathcal{L}(s) = \mathbb{E}\left[e^{sS}\right] = \mathbb{E}\left[exp\left(-\sum_{\mathbf{x} \in \Phi} s f(x)\right)\right] = exp\left(-\lambda \int_{\mathbb{R}^2} (1 - e^{-sf(x)}) dx\right). \quad (2.1)$$

If the desired signal power is exponentially distributed, i.e. Rayleigh fading, calculation of coverage probability which depends on SINR requires the computation of Laplace transform of the interference measured at the receiver, hence PGFL of a PPP will be used widely in the following sections.

2.2. Properties of PPP

(i) Independent thinning of a PPP

Let $g : \mathbb{R}^d \to [0, 1]$ be a thinning function of a stationary PPP Φ by independently deleting each point x with a probability $1 - g(x)$. This will end up with an inhomogeneous PPP with intensity function $\lambda g(x)$.

This thinning feature is one of the most useful properties of PPP while calculating the ICIC effect on coverage probability.

(ii) Superposition of PPP

Superposition of independent PPPs end up in a PPP. Hence, combination of n independent homogeneous PPPs with intensities $\lambda_i, i = 1, 2, ..., n$ form a new PPP with intensity $\sum_{i=1}^{n} \lambda_i$.

(iii) Displacement Theorem

The transformation of the PPP of intensity measure Λ by a probability kernel p is the PPP with intensity measure $\Lambda'(A) = \int_{\mathbb{R}^d} p(x, A)\Lambda(dx)$.

As a result, we can conclude that independent displacements preserve PPP property. In [51], it is shown that displacement under random walk and random waypoint model preserves the Poisson property and it leads to independence between Φ (initial PPP) and Φ' (displaced PPP) if the initial PPP has an intensity measure which is 0 outside a finite window.

(iv) Stationarity

A point process Φ is stationary if its distribution is invariant under translation through any vector $v \in \mathbb{R}^d$.

As a special case of this lemma, one can easily conclude that a homogeneous PPP (i.e. with a constant intensity measure λ) is stationary. In addition to this, homogeneous PPP is erdogic.

We will mainly focus on a homogeneous PPP, which is a PPP with uniform intensity λ such that mean $\mu(A) = \lambda l(A)$, where $l(A)$ is a Lebesgue measure of A. As a result of the property of a homogeneous PPP, all the points are independently and uniformly distributed in A, conditioning on the number of points in A.

2.3. Palm Theory

In the study of point processes of wireless networks, it is often natural to condition on a point at the fixed location. Palm theory gives description for the notion of the conditional distribution of a general point process which contains a point at some location. Since the probability of the condition is equal to 0 for a point process without a fixed atom at this particular location, the basic definition of the conditional probability is not applicable. It also formalizes the concept of the typical point which has the same probability of being chosen in the random selection procedure. The palm distribution is the conditional point process distribution provided that a typical point exists at a specific location.

A chosen point that is the closest to the origin is not typical, because of a selection in a deterministic way. For instance, assume that we want to calculate the SINR of a desired transmitter, the other node will be interferers. When we condition on the location of the desired transmitter, it should not be treated as an interferer and its effect should be eliminated in the calculations. This example leads to a reduced Palm distribution if all the transmitting nodes constitute a point process.

One of the main consequences of Palm theory for PPP leads to Slivnyak–Mecke theorem, which has a powerful effect on reduced Palm distributions. The interested reader can refer to [51] to go over the proof of the theorem.

Definition 2.3.1. Slivnyak-Mecke theorem

Let Φ be a PPP with intensity measure Λ. For almost all $x \in \mathbb{R}^d$,

$$P_x^!(\cdot) = \mathbb{P}\{\Phi \in \cdot\}$$

where $P_x^!$ is the reduced Palm distribution of PPP and it is equal to its original distribution.

As a consequence of this theorem and the independence property of the PPP, the number of points in $B(x, \epsilon)$ is independent of the number of points in any region outside this ball, for arbitrary small ϵ. This suggests that conditioning on a point x does not change the distribution of the rest of the process and it allows us to add a node into the region at any location, such as the origin or at a fixed distance from the origin, without changing its statistical properties. It enables us to consider the interference as coming from a PPP, even though we exclude the serving BS from PPP.

3. COVERAGE PROBABILITY ANALYSIS FOR SINGLE-TIER OFDMA CELLULAR NETWORKS

In this chapter, we will provide both the theoretical and simulation analyses of the single-tier network by applying ICIC techniques that we have mentioned in the Chapter 1. Stochastic geometry tools and point process theory that are outlined previously form the backbone of our analysis for coverage probability, which is one of the key performance metrics of the cellular networks.

Unlike the traditional hexagonal grid model, the location of the base stations are distributed as a homogeneous Poisson point process (PPP) with density λ for an OFDMA cellular downlink transmission. This brings some sort of randomness which helps to capture the nonuniform map of the recent cellular deployments due to topographic or demographic effects.

In the general framework, coverage probability is defined as the probability of the instantaneous SINR of a user which is greater than specified SINR threshold and given by

$$p_c = \mathbb{P}(SINR > T) \tag{3.1}$$

which is equivalent of complementary cumulative distribution function (CCDF) of the SINR.

Assuming there is Rayleigh fading between any BS z and the typical user y, fading value g_z is exponentially distributed with mean μ. Z represents the group of interfering BSs, which use the same subband as user y. R_z represents the distance between the interfering BS z and the typical user, where α, σ^2, Δ denotes pathloss exponent, the noise power and number of frequency sub-bands respectively. We also assume that all the BSs have the same transmit power P. The SINR of the mobile user at a random

distance r from its tagged BS can be expressed by

$$SINR = \frac{Pg_y r^{-\alpha}}{\sigma^2 + PI_r}, \tag{3.2}$$

where

$$I_r = \sum_{z \in Z} g_z R_z^{-\alpha}. \tag{3.3}$$

Assumption in the above formula is that the nearest BS to the user y is located at a distance r, which is a random variable. By using the null probability of a 2-D PPP in a given area, the probability density function (pdf) of r can be calculated by

$$f_r(r) = e^{-\lambda \pi r^2} 2\pi\lambda r dr. \tag{3.4}$$

In Andrews et al.'s well-known work [21], the general expression for coverage probability in the presence of exponential interference is derived as

$$p_c(T, \lambda, \alpha, r) = \pi\lambda \int_0^\infty e^{-\pi\lambda v(1+\frac{1}{\Delta}\rho(T,\alpha)) - \mu T\sigma^2 v^{\alpha/2}} dv, \tag{3.5}$$

where

$$\rho(T, \alpha) = T^{2/\alpha} \int_{T^{-2/\alpha}}^\infty \frac{1}{1 + u^{\alpha/2}} du. \tag{3.6}$$

Use of strict FFR and SFR divides users into two categories: edge and interior users. Unlike deterministic grid models, the PPP model uses SINR levels in order to classify the users instead of constant distances and it does not give the same geographic meaning. Each cell is divided into Voronoi regions with a random area, resulting in a more realistic image of actual deployments of recent mobile cellular networks. If SINR

is less than a frequency reuse threshold T_{FR}, users are defined as edge users, while users whose SINR is greater than T_{FR} are categorized as interior users. Hence, T_{FR} can be considered as an analogous design parameter of the grid-based interior radius [52].

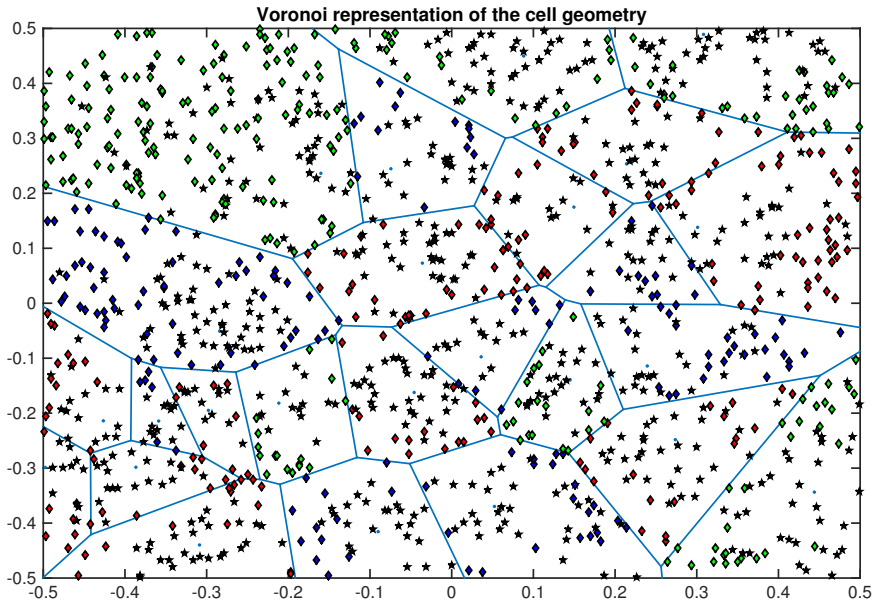

Figure 3.1. Voronoi regions of the network topology.

Figure 3.1 delineates a snapshot of the network topology which is composed of Voronoi regions under frequency reuse scheme. Users that are represented with a diamond shape are cell-edge users, while users that are showed by a pentagram shape are interior users as defined above. Different colors (i.e. red, green and blue) represent different frequency subbands.

3.1. Strict FFR Edge User

In the case of strict FFR, if SINR of a user goes below the reuse threshold T_{FR}, user is allocated a new subband from reserved subbands for the edge users as a result of the reuse strategy. User y with $SINR < T_{FR}$ is assigned a new FFR subband δ_y, where $\delta \in 1, ..., \Delta$ with uniform probability $\frac{1}{\Delta}$. This results in a new fading power $\hat{g}$ and out-of-cell interference $\hat{I}$, which are different than initial g_y and I_r, respectively. Assuming $\hat{g}$ and g are i.i.d. exponentially distributed with mean μ, the CCDF of the edge user $F_{FFR}(T)$ is calculated in [23] by

$$F_{FFR}(T) = \mathbb{P}\left(\frac{P\hat{g}r^{-\alpha}}{\sigma^2 + P\hat{I}_r} > T \middle| \frac{Pgr^{-\alpha}}{\sigma^2 + PI_r} < T_{FR}\right)$$
$$= \frac{p_c(T,\lambda,\alpha,\Delta) - \pi\lambda \int_0^\infty e^{-\pi\lambda v(1+2\xi(T,T_{FR},\alpha,\Delta)) - \mu(T+T_{FR})\frac{\sigma^2}{P}\upsilon^{\alpha/2}} d\upsilon}{1 - p_c(T_{FR},\lambda,\alpha,1)} \tag{3.7}$$

where

$$\xi(T,T_{FR},\alpha,\Delta) = \int_1^\infty \left[1 - \frac{1}{1+T_{FR}x^{-\alpha}}\left(1 - \frac{1}{\Delta}\left(1 - \frac{1}{1+Tx^{-\alpha}}\right)\right)\right] xdx \tag{3.8}$$

and p_c is given by (3.5). Proof can be found in the appendix section A.1. This proof will form the basis for the analyses in the following sections.

If we consider the special case where $\alpha = 4$, we can obtain an insight about the performance of cell-edge users by obtaining closed form expressions for the coverage probability, instead of computing complex integrals.

3.1.1. Special Case: α =4

When $\alpha = 4$, $\xi(T,T_{FR},\alpha,\Delta)$ turns into a closed form trigonometric equation instead of a numerically evaluated integral, whose derivation is given in A.2. It can be calculated according to the following formula,

$$\xi(T,T_{FR},4,\Delta) = \frac{T\rho(T,4) - \rho(T_{FR},4)(T_{FR}\Delta - T(\Delta-1))}{2\Delta(T-T_{FR})} \tag{3.9}$$

where

$$\rho(T,4) = \sqrt{T}arctan(\sqrt{T}). \tag{3.10}$$

3.1.2. Special Case: No noise and α =4

If the given network is only an interference-limited network in which noise is neglected, coverage probability of strict FFR edge user can be computed by

$$F_{FFR}(T) = \frac{1+\rho(T_{FR},4)}{\rho(T_{FR},4)}\left(\frac{1}{1+\frac{1}{\Delta}\rho(T_{FR},4)} - \frac{1}{1+2\xi(T,T_{FR},4,\Delta)}\right) \tag{3.11}$$

where $\xi(T,T_{FR},4,\Delta)$ is given in (3.9). Distribution of SINR in (3.11) is a function of only the SINR threshold T and the reuse threshold T_{FR} under this special case.

3.2. SFR Edge User

In the case of SFR, I_r comes from two different categories where $P_{int} = P$ and $P_{edge} = \beta P$ with a power control factor $\beta \geq 1$, unlike the case of strict FFR. P_{int} is the transmit power of the BS for an interior user and P_{edge} is the transmit power of the BS for an edge user. As a result, the interfering BSs are divided into two categories as well: I_{int}, which is caused by all the interfering BSs that transmit to interior users on the same subband of a typical user y with a power of $P_{int}$and I_{edge}, which is caused by all the interfering BSs that transmit to edge users on the same subband of user y with a power of P_{edge}. Hence, total out-of-cell interference with SFR is

$$I_r = \sum_{i\in I_{int}} g_i R_i^{-\alpha} + \beta \sum_{i\in I_{edge}} g_i R_i^{-\alpha}. \tag{3.12}$$

Main difference between strict FFR and SFR is the use of power control factor, β. BSs are allowed to reuse all subbands by applying β to one of the δ subbands of edge users. Therefore, the effective interference power factor η can be found by $\eta = (\Delta - 1 + \beta)/\Delta$ and the overall interference term is defined by $\eta P I_r$.

User y with $SINR < T_{FR}$ is given a new SFR sub-band δ_y, where $\delta \in 1, ..., \Delta$ with a transmit power of βP. This results in a new fading power $\hat{g}$ and out-of-cell

interference $\hat{I}$, which are different than initial g_y and I_r, respectively. Assuming $\hat{g}$ and g are i.i.d. exponentially distributed with mean μ , the CCDF of the edge user $F_{SFR}(T)$ is calculated in [23] by

$$\begin{aligned} F_{SFR}(T) &= \mathbb{P}\left(\frac{\beta P\hat{g}r^{-\alpha}}{\sigma^2+\eta P\hat{I}_r} > T \middle| \frac{Pgr^{-\alpha}}{\sigma^2+\eta PI_r} < T_{FR}\right) \\ &= \frac{p_c(\eta\frac{T}{\beta},\lambda,\alpha,\Delta) - \pi\lambda\int_0^\infty e^{-\pi\lambda v(1+2\zeta(T,T_{FR},\alpha,1,\eta,\beta))-\mu(\eta\frac{T}{\beta}+\eta T_{FR})\frac{\sigma^2}{P}v^{\alpha/2}}dv}{1-p_c(\eta T_{FR},\lambda,\alpha,1)} \end{aligned} \tag{3.13}$$

where

$$\zeta(T,T_{FR},\alpha,1,\eta,\beta) = \int_1^\infty \left[1 - \frac{1}{1+\eta T_{FR}x^{-\alpha}}\frac{1}{1+\eta\frac{T}{\beta}x^{-\alpha}}\right] xdx. \tag{3.14}$$

Similarly, as in the case of strict FFR, if we consider the special case where $\alpha = 4$, we can obtain an insight about the performance of cell-edge users by obtaining closed form expressions for the coverage probability.

3.2.1. Special Case: α=4

When $\alpha = 4$, $\zeta(T,T_{FR},4,\eta,\beta)$ turns into a closed form trigonometric equation instead of a numerically evaluated integral, which can be found by

$$\zeta(T,T_{FR},4,\eta,\beta) = \frac{1}{2(T-\beta T_{FR})}\left(T\rho(\frac{\eta}{\beta}T,4) - \beta T_{FR}\rho(\eta T_{FR},4)\right) \tag{3.15}$$

where $\rho(T,4)$ is given in (3.10).

3.2.2. Special Case: No noise and $\alpha = 4$

If interference-limited network in which noise is neglected, is considered, coverage probability of SFR edge user can be computed by

$$F_{SFR}(T) = \frac{1+\rho(\eta T_{FR}, 4)}{\rho(\eta T_{FR}, 4)} \left(\frac{1}{1+\rho(\frac{\eta}{\beta}T, 4)} - \frac{1}{1+2\zeta(T, T_{FR}, \alpha, \eta, \beta)} \right) \tag{3.16}$$

where $\zeta(T, T_{FR}, \alpha, \eta, \beta)$ is given in (3.15).

Distribution of SINR in (3.16) is a function of the certain design parameters, namely power control factor β, the reuse threshold T_{FR} and the SINR threshold T.

3.3. Simulation Results

The parameters and corresponding values which are used in order to obtain MATLAB simulation results of a single-tier network system are summarized in Table 3.1.

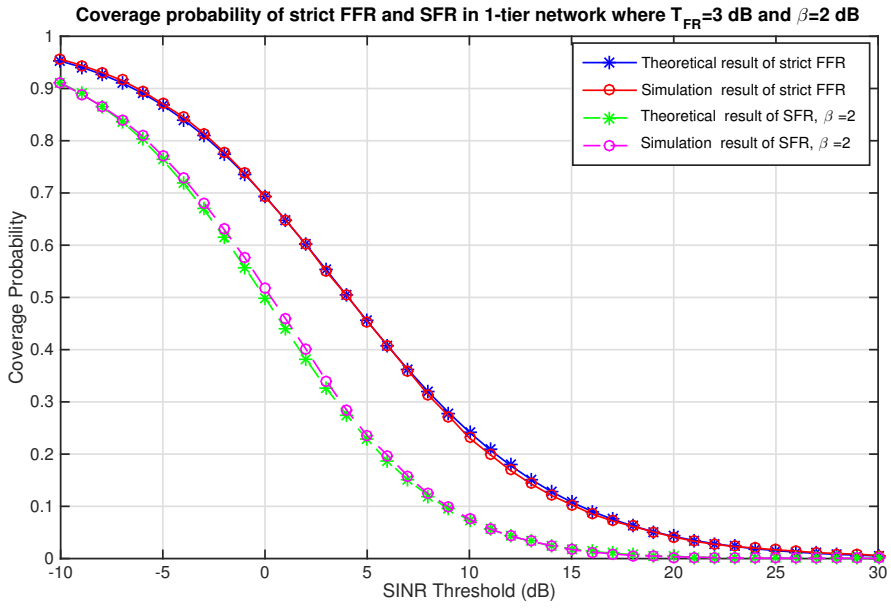

Figure 3.2. Coverage probability of strict FFR and SFR in 1-tier network with 3 dB FFR threshold and power factor=2 when there is no noise and $\alpha = 4$.

Table 3.1. Simulation parameters for single-tier network.

Parameter	Value / Assumption
Cell geometry	Voronoi
BS distribution	PPP
BS density (λ)	$1/4000\pi$ BSs/m^2
User distribution	PPP
User density (λ_u)	0.01 $users/m^2$
Edge user threshold	3 dB
Pathloss exponent (α)	4
Total number of subbands	48
Reuse factor (Δ)	3
Frequency planning	Strict FFR SFR
Power Control Factor (β)	2 dB

Figure 3.2 depicts the simulation and theoretical results of the coverage probabilities under strict FFR and SFR schemes where the reuse threshold $T_{FR} = 3$ dB and power control factor $\beta = 2$ dB. This results show that our simulation environment provides consistent results with the results from theoretical calculations. As noted before, it can be observed that strict FFR provides more improvement in mitigation of the interference compared to SFR at the expense of spectral efficiency.

3.4. Conclusion

In this chapter, we provide the Monte Carlo simulation results of coverage probability of the edge users in a single-tier network, which are verified by analytical results. The simulated results when node and user distributions follow a PPP, consistently match the theoretical analysis for both strict FFR and SFR techniques as seen in Figure 3.2. We extend these analyses to heterogeneous networks in the next chapter.

4. COVERAGE PROBABILITY ANALYSIS FOR HETEROGENEOUS NETWORKS

We consider downlink of a heterogeneous cellular network which is composed of k types of BSs, which may consist of macro, pico and femtocells, with different transmit power, intensity and target SINR threshold. Some sort of interference mitigation method becomes more essential in HetNets, since these tiers are overlapping in many cases and HetNets rapidly approach the interference limits for a satisfactory QoS. Figure 4.1 depicts the frequency and transmit power allocation with $\Delta = 3$ under FFR and SFR schemes. As can be seen in Figure 4.1, strict FFR provides a significant mitigation in the interference for cell-edge users at the cost of spectral efficiency. Since the subbands of the edge users in other cells can be allocated to the interior users as well, SFR scheme utilizes all Δ subbands by using power control factor β for edge users.

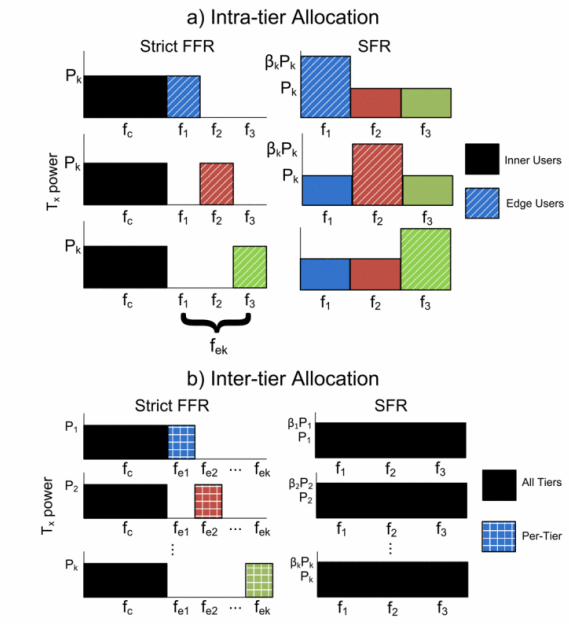

Figure 4.1. a) Intra-tier subband and transmit power allocations under strict FFR and SFR. b) Inter-tier subband allocations for the case in which frequency reuse factor $\Delta = 3$ for all tiers [3].

An independent homogeneous PPP Φ_k with intensity λ_k is used to model BS locations of the k^{th} tier. Assuming that all the BSs of the k^{th} tier transmit at the same power P_k and T_k represents target SINR threshold for the k^{th} tier, k^{th} tier can be characterized fully by $\{\lambda_k, P_k, T_k\}$.

For the sake of simplicity, i.i.d. Rayleigh fading is assumed in our analyses, the received signal power of a user from an k^{th} tier BS at a distance r is calculated by $P_k g_k r_k^{-\alpha}$, where $g_k \sim exp(1)$. As a result, SINR of the user who is associated to the k^{th} tier BS which is located at $\mathbf{X_k} \in \Phi_k$ is

$$SINR(\mathbf{X_k}) = \frac{P_k g_k r_k^{-\alpha}}{\sum_{j=1}^{K} \sum_{\mathbf{X} \in \Phi_j \setminus \mathbf{X_k}} P_j g_j r_j^{-\alpha} + \sigma^2} = \frac{P_k g_k r_k^{-\alpha}}{\sum_{j \neq k}^{K} I_j + \sigma^2} \tag{4.1}$$

where $I_{(\Phi \setminus \{\mathbf{X_i}\})}$ represents the interference and σ^2 denotes the additive noise power. In a network, which consists of one type of BS only, users are assigned to the closest BS in terms of Euclidean distance, resulting in Poisson-Voronoi tessellation. However, this tessellation is not valid for HetNets because of the differences in the transmit powers of the BSs across tiers and the corresponding fading. Hence, the closest BS from each tier is not necessarily the serving BS. For this case, weighted Voronoi diagram should be used to represent this tessellation model in HetNets, which depends on the maximum average received power. Figure 4.2 demonstrates an example of weighted Voronoi diagram in HetNets.

There are two main spectrum access strategies for small cells in a HCN, namely open-access and closed-access policies. In an open-access strategy, all cellular users (subscribers and non-subscribers) have a right to take a service from small cells. In a closed-access strategy, only subscribed cellular users are authorized to take a service by small cells.

Open-access policy reinforces the overall network coverage and mean transmission rate but does not ensure the QoS for a subscribed small cell users [53]. On the other hand, closed-access policy may lead to degradation in performance of non-subscriber

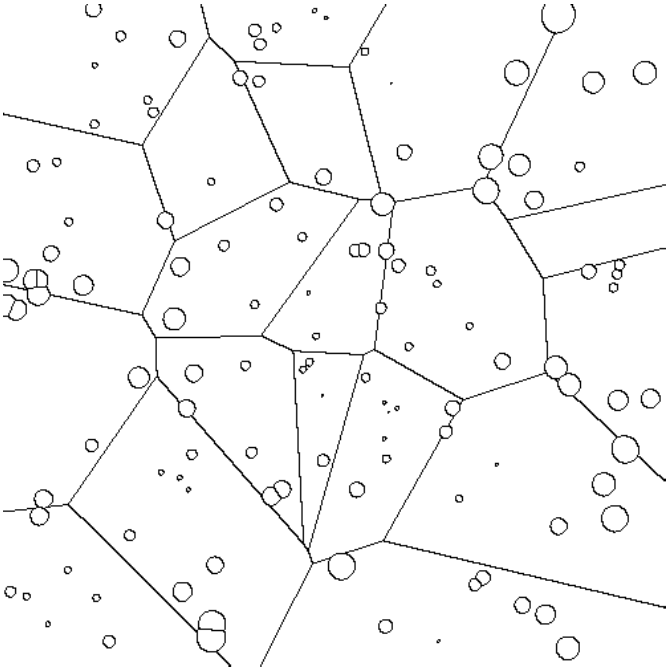

Figure 4.2. Weighted Voronoi.

cellular users, in return for ensuring the QoS for the subscribed users in the closed access policy. It is worth mentioning that closed access subscribed users may also suffer from significant interference caused by the non-subscribed users [25].

4.1. Closed Access Case in HetNets

As stated previously, only subscribed cellular users that are licensed are allowed to be served by small cells in the closed-access strategy. Consider a two-tier network as an example and assume that a mobile user who is connected to the macrocell BS may be in the range of a femtocell. Since the user is unable to connect to that femtocell, user may potentially cause a serious cross-tier interference for other users, whereas the closed access policy provides a good coverage and satisfactory QoS for the subscribed users.

4.1.1. Strict FFR Edge User

Under strict FFR technique, SINR of the user for the closest BS of the k^{th} tier is determined first and if the SINR goes below the tier's FFR threshold T_k, the user is categorized as an exterior user and is allocated a new subband from reserved subbands Δ_k for the cell-edge users with uniform probability $\frac{1}{\Delta}$. This results in a new out-of-cell interference $P_k\hat{I}_k$ and fading power $\hat{g_k}$. Assuming $\hat{g}$ and g_k are i.i.d. exponentially distributed with mean μ, and following the similar approaches in the previous section, the CCDF of the cell-edge user $F_{FFR,cl}(T)$ can be calculated by

$$F_{FFR,cl}(k,T) = \frac{\pi\lambda_k \int_0^\infty e^{-\pi\lambda_k \upsilon(1+\frac{\rho(T_k,\alpha)}{\Delta_k})} e^{-\mu(T+T_k)\frac{\sigma^2}{P_k}\upsilon^{\alpha/2}} d\upsilon}{f_{den}} - \frac{\pi\lambda_k \upsilon \int_0^\infty e^{-\pi\lambda_k \upsilon(1+2\xi(T,T_k,\alpha,\Delta_k))} e^{-2\pi\lambda_k \upsilon(\sum_{j\neq k}^K \kappa_{j,k}\psi(\gamma_{j,k}T_k,\alpha))} e^{-\mu(T+T_k)\frac{\sigma^2}{P_k}\upsilon^{\alpha/2}} d\upsilon}{f_{den}} \tag{4.2}$$

where

$$f_{den} = 1 - \pi\lambda_k \int_0^\infty e^{-\pi\lambda_k \upsilon(1+\rho(T_k,\alpha))} e^{-2\pi\lambda_k \upsilon(\sum_{j\neq k}^K \kappa_{j,k}\psi(\gamma_{j,k}T_k,\alpha))} e^{-\mu(T+T_k)\frac{\sigma^2}{P_k}\upsilon^{\alpha/2}} d\upsilon \tag{4.3}$$

and

$$\xi(T,T_k,\alpha,\Delta_k) = \int_{r_k}^\infty \left[1 - \frac{1}{1+T_k r_k^\alpha x^{-\alpha}}\left(1 - \frac{1}{\Delta_k}\left(1 - \frac{1}{1+T r_k^\alpha x^{-\alpha}}\right)\right)\right] x dx \tag{4.4}$$

and

$$\psi(z,\alpha) = \frac{\pi z^{2/\alpha}}{\alpha} csc(\frac{2\pi}{\alpha}), \gamma_{j,k} = \frac{P_j}{P_k}, \kappa_{j,k} = \frac{\lambda_j}{\lambda_k}. \tag{4.5}$$

Proof is provided in the appendix section A.3. It should be noted that this derived equation is formed by the function which uses corresponding strict FFR parameters as an input. $\xi(T,T_k,\alpha,\Delta_k)$ term contains the intra-tier interference before the strict FFR is employed, whereas $\rho(z,\alpha)$ terms contains the intra-tier interference after the strict

FFR is employed. Moreover, $\psi(z, \alpha)$ accommodates the terms that are related to the cross-tier interference for each tier.

Consideration of the special case where $\alpha = 4$ provides a good intuition about the performance of the cell-edge users of HetNets by simplifying the equations and obtaining the closed form expressions for the coverage probability.

Special Case: α =4.

When $\alpha = 4$, $\xi(T, T_k, \alpha, \Delta)$ turns into a closed form trigonometric equation instead of an integral that is

$$\xi(T, T_k, 4, \Delta) = \frac{T\rho(T) - \rho(T_k)(T_k\Delta - T(\Delta - 1))}{2\Delta(T - T_k)} \tag{4.6}$$

and

$$\psi(z, 4) = \frac{\pi\sqrt{z}}{4}. \tag{4.7}$$

Special Case: No noise and α =4.

If interference-limited network in which noise is neglected, is considered, coverage probability becomes

$$\begin{aligned} F_{FFR,cl}(k, T) = & \frac{1 + \rho(T_k, 4) + \frac{\pi}{2}\sum_{j\neq k}^{K} \kappa_{j,k}\sqrt{\gamma_{j,k}T_k}}{\rho(T_k, 4) + \frac{\pi}{2}\sum_{j\neq k}^{K} \kappa_{j,k}\sqrt{\gamma_{j,k}T_k}} \times \\ & \left(\frac{1}{1 + \frac{\rho(T_k,4)}{\Delta_k}} - \frac{1}{1 + 2\xi(T, T_k, 4, \Delta) + \frac{\pi}{2}\sum_{j\neq k}^{K} \kappa_{j,k}\sqrt{\gamma_{j,k}T_k}}\right) \end{aligned} \tag{4.8}$$

where $\xi(T, T_k, 4, \Delta)$ is given in (4.6).

4.1.2. SFR Edge User

After following the similar approaches in the strict FFR case, coverage probability of SFR cell-edge users under closed access scheme can be computed by

$$F_{SFR,cl}(k,T) = \frac{\pi\lambda_k \int_0^\infty e^{-\pi\lambda_k \upsilon(1+\rho(\frac{\eta_k T}{\beta_k},\alpha)+2\sum_{j\neq k}^{K}\kappa_{j,k}\psi(\frac{\gamma_{j,k}T}{\beta_k},\alpha))} e^{-\mu T\frac{\sigma^2}{\beta_k P_k}\upsilon^{\alpha/2}} d\upsilon}{f_{s,den}} - \frac{\pi\lambda_k \int_0^\infty e^{-\pi\lambda_k \upsilon(1+2\zeta(T,T_k,\alpha,\beta_k,\eta_k))} e^{-2\pi\lambda_k \upsilon(\sum_{j\neq k}^{K}\kappa_{j,k}(\psi(\frac{\beta_j\gamma_{j,k}T_k}{\beta_k},\alpha)+\psi(\gamma_{j,k}T_k,\alpha))} e^{-\mu(T+\eta_k T_k)\frac{\sigma^2}{P_k}\upsilon^{\alpha/2}} d\upsilon}{f_{s,den}} \tag{4.9}$$

where

$$f_{s,den} = 1-\pi\lambda_k \int_0^\infty e^{-\pi\lambda_k \upsilon(1+\rho(\eta_k T_k,\alpha))} e^{-2\pi\lambda_k \upsilon(\sum_{j\neq k}^{K}\kappa_{j,k}\psi(\gamma_{j,k}T_k,\alpha))} e^{-\mu(\eta_k T_k)\frac{\sigma^2}{P_k}\upsilon^{\alpha/2}} d\upsilon \tag{4.10}$$

and

$$\zeta(T,T_k,\alpha,\beta_k,\eta_k) = \int_1^\infty \left[1 - \frac{1}{1+\eta_k T_k x^{-\alpha}} \frac{1}{1+\eta_k \frac{T}{\beta_k} x^{-\alpha}}\right] x dx \tag{4.11}$$

and $\psi(z,\alpha), \gamma_{j,k}, \kappa_{j,k}$ are given in (4.5).

Special Case: α =4.

When $\alpha = 4$, $\zeta(T,T_k,\alpha,\Delta)$ turns into a closed form trigonometric equation instead of an integral, that is

$$\zeta(T,T_k,\alpha,\beta_k,\eta_k) = \frac{1}{2(T-\beta T_k)} \left(T\rho(\frac{\eta}{\beta}T) - \beta T_k \rho(\eta T_k)\right). \tag{4.12}$$

Special Case: No noise and α =4.

If interference-limited network, i.e. noise is neglected, is considered, coverage probability reduces to

$$F_{SFR,cl}(k,T) = \frac{1+\rho(\eta_k T_k,4)+\frac{\pi}{2}\sum_{j\neq k}^{K}\kappa_{j,k}\sqrt{\gamma_{j,k}T_k}}{\rho(\eta_k T_k,4)+\frac{\pi}{2}\sum_{j\neq k}^{K}\kappa_{j,k}\sqrt{\gamma_{j,k}T_k}} \times \left(\frac{1}{1+\frac{\rho(\frac{\eta_k T_k}{\beta_k},4)+}{\Delta_k}+\frac{\pi}{2}\sum_{j\neq k}^{K}\sqrt{\frac{\gamma_{j,k}}{\beta_k}T_k}} - \frac{1}{1+2\zeta(T,T_k,4,\beta_k,\eta_k)+\frac{\pi}{2}\sum_{j\neq k}^{K}\kappa_{j,k}\sqrt{\gamma_{j,k}T_k}}\right) \tag{4.13}$$

where $\zeta(T,T_k,4,\beta_k,\eta_k)$ is given in (4.12).

4.1.3. Simulation Results

The parameters employed in order to get Monte Carlo simulation results of a two-tier network system with a closed access scheme are summarized in Table 4.1.

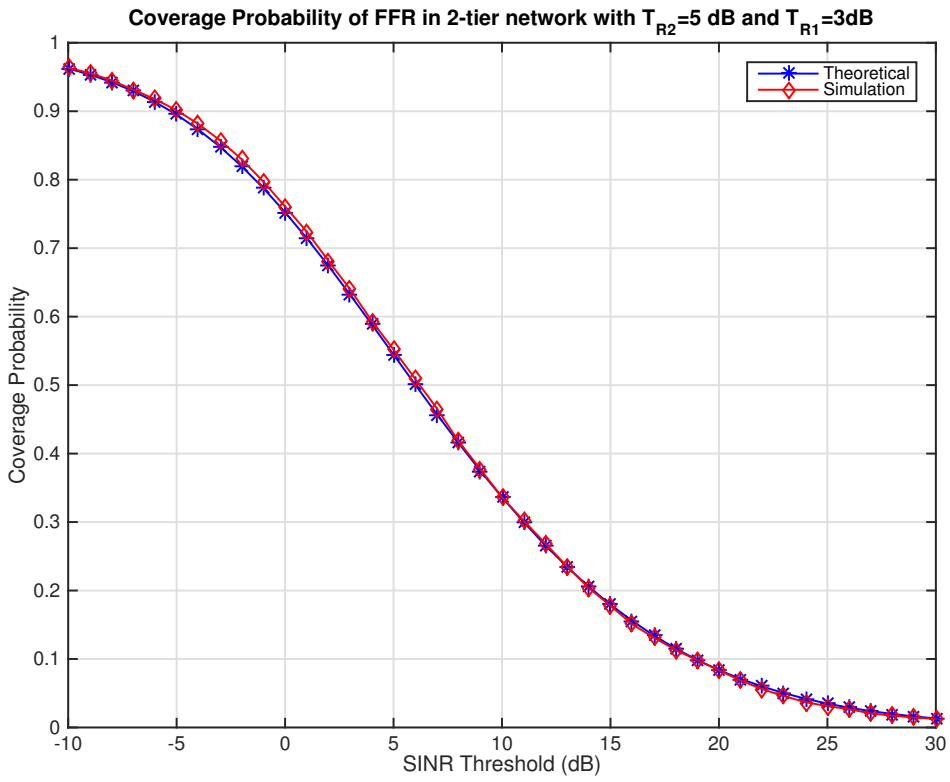

Figure 4.3. Coverage probability of strict FFR in a 2-tier network under closed access scheme with $T_1 = 3$ dB, $T_2 = 5$ dB FFR threshold when there is no noise and $\alpha = 4$.

Table 4.1. Simulation parameters for a heterogeneous network with a closed access policy.

Parameter	Value / Assumption
Cell geometry	Weighted Voronoi
BS distribution	PPP
Macro BS density (λ_1)	$1/4000\pi$ BSs/m^2
Femto BS density (λ_2)	$1/500\pi$ BSs/m^2
Density ratio (κ_{21})	8
Power ratio (γ_{21})	0.001
User distribution	PPP
User density (λ_u)	0.01 $users/m^2$
Edge user SINR threshold of macrocells	3 dB
Edge user SINR threshold of femtocells	5 dB
Pathloss exponent (α)	4
Number of subbands	48
Reuse factor (Δ)	3
Frequency planning	Strict FFR SFR
Power control factor (β)	2,4,8,16 dB
Access scheme	Closed access

The simulation and theoretical results of the coverage probability of the first tier (i.e. macrocell) in a 2-tier network under closed access scheme with use of strict FFR are shown in Figure 4.3. The reuse threshold for macrocells is chosen as $T_1 = 3$ dB, whereas the reuse threshold of femtocells is selected as $T_2 = 5$ dB.

Figure 4.4 compares the coverage probabilities of the macrocells in a single tier and 2-tier networks. It is important to observe that adding femtocells to the network improves the SINR quality up to 3 dB under the given parameters for the same level of coverage probability. As a result, introducing small cells with the lower transmit

power into the network provides successful solution to degradation in the performance of the network caused by the interference.

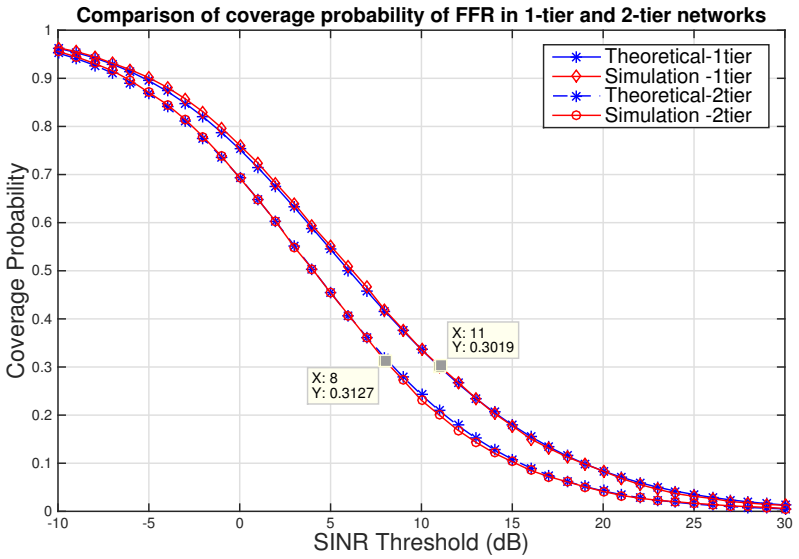

Figure 4.4. Comparison of coverage probabilities of FFR in 1-tier and 2-tier networks when there is no noise and $\alpha = 4$.

Figure 4.5 presents the related simulation results for SFR under closed access scheme for different values of power control factor β. This results show that our simulation environment provides consistent results with the results from theoretical calculations.

4.2. Open Access Strategy

In a network with the open access strategy, a user is granted permission to take a service from any BS in the network without any restriction. Therefore, this method provides a better performance in terms of SINR and the coverage probability in comparison to the closed access assignment policy. For the sake of the simplicity in the calculations, we assume that the network consists of two tiers of BSs and it is an interference-limited network, in which SIR is used as the performance metric in the following analysis of performance of open access scheme.

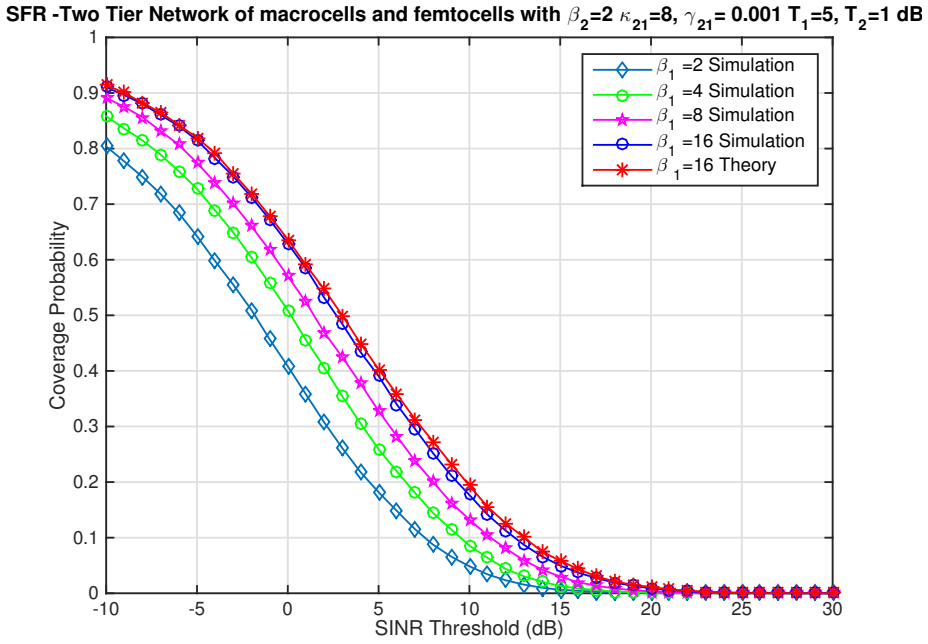

Figure 4.5. Coverage probability of SFR in two-tier network of macrocells and femtocells with $\beta_2 = 2\kappa_{21} = 8, \gamma_{21} = 0.001, T_1 = 5, T_2 = 1$ dB when there is no noise and $\alpha = 4$.

As a result, SIR for the first tier and SIR for the second tier can be defined by

$$SIR_1 = \frac{P_1 g_1 r_1^{-\alpha}}{P_1 I_1 + P_2 I_2 + P_2 g_2 r_2^{-\alpha}} \tag{4.14}$$

$$SIR_2 = \frac{P_2 g_2 r_2^{-\alpha}}{P_1 I_1 + P_2 I_2 + P_1 g_1 r_1^{-\alpha}} \tag{4.15}$$

where r_1 represents the distance between the mobile user at the center and the closest first tier BS, and r_2 represents the distance between the mobile user at the center and the closest second tier BS. I_1 denotes the interference due to the first tier BSs, while I_2 denotes the interference due to the second tier BSs, except for the nearest BS.

This case brings more complicated equations than the closed access system because of the interdependent relation of the terms SIR_1 and SIR_2. For a notational convenience, the first-tier edge user SIR are considered in the following theorems of

this section and simulation results for the first tier are presented at the end of this section. However, theorems and simulations can be easily adapted to the second-tier cell-edge users.

4.2.1. Strict FFR Edge User

According to open access policy under strict FFR scheme, a cellular user is assigned a different FFR subband δ_y, with $1/\Delta$ uniform probability, if $SIR_1 < T_1$ and $SIR_2 < T_2$, where T_1 is the open access threshold for the first tier BSs and T_2 is the open access threshold for the second tier APs. The new SIR after this assignment is calculated by $S\hat{I}R = \frac{P_1 \hat{g_1} r_1^{-\alpha}}{P_1 \hat{I_1}}$ for the first tier SIR and the coverage probability of the cell-edge user under open access method can be calculated by

$$\begin{aligned} F_{FFR,open,edge}(T) &= \mathbb{P}\left(S\hat{I}R > T | SIR_1 < T_1, SIR_2 < T_2\right) \\ &= \frac{f_n(r_1, r_2)}{f_d(r_1, r_2)} \end{aligned}$$

where

$$\begin{aligned} f_d(r_1, r_2) = 1 - \epsilon_1 \int_0^\infty 2\pi\lambda_1 r_1 e^{-2\pi\lambda_1 r_1^2(\rho_1(T_1,\alpha)+1+\kappa\psi(\gamma T_1,\alpha))} dr_1 + \\ (\epsilon_2 - 1) \int_0^\infty 2\pi\lambda_2 r_2 e^{-2\pi\lambda_2 r_2^2(\rho_2(T_2,\alpha)+1+\frac{1}{\kappa}\psi(\frac{T_2}{\gamma},\alpha))} dr_2 \end{aligned} \tag{4.16}$$

with

$$\begin{aligned} \rho_1(T_1, \alpha) &= \int_{r_1}^\infty \left(1 - \frac{1}{1 + T_1 r_1^\alpha x^{-\alpha}}\right) x dx \\ \rho_2(T_2, \alpha) &= \int_{r_2}^\infty \left(1 - \frac{1}{1 + T_2 r_2^\alpha x^{-\alpha}}\right) x dx \\ \psi(z, \alpha) &= \frac{\pi z^{2/\alpha}}{\alpha} csc(\frac{2\pi}{\alpha}) \\ \gamma = \frac{P_2}{P_1}, \kappa &= \frac{\lambda_2}{\lambda_1} \end{aligned}$$

and

$$f_n(r_1,r_2)=p_c(T,\lambda_1,\alpha,\Delta)-\epsilon_1\left(\int_0^\infty 2\pi r_1\lambda_1 e^{-\pi\lambda_1 {r_1}^2(1+\xi_1(T,T_1,\alpha,\Delta))}e^{-2\pi\lambda_1 {r_1}^2\kappa\psi(\gamma T_1,\alpha)}dr_1\right)$$
$$+(\epsilon_2-1)\left(\int_0^\infty\int_0^\infty 2\pi r_1\lambda_1 2\pi r_2\lambda_2 e^{-\pi\lambda_1 {r_1}^2(1+\xi_2(T,T_2/\gamma,\alpha,\Delta))}e^{-2\pi\lambda_2 {r_2}^2(1+\frac{1}{\kappa}\psi(T_2/\gamma,\alpha))}dr_1dr_2\right) \tag{4.17}$$

with

$$\xi_1(T,T_1,\alpha,\Delta)=\int_{r_1}^\infty\left[1-\frac{1}{1+T_1r_1^\alpha x^{-\alpha}}\left(1-\frac{1}{\Delta}\left(1-\frac{1}{1+Tr_1^\alpha x^{-\alpha}}\right)\right)\right]xdx \tag{4.18}$$

$$\xi_2(T,\frac{T_2}{\gamma},\alpha,\Delta)=\int_{r_1}^\infty\left[1-\frac{1}{1+(\frac{T_2}{\gamma})r_2^\alpha x^{-\alpha}}\left(1-\frac{1}{\Delta}\left(1-\frac{1}{1+Tr_1^\alpha x^{-\alpha}}\right)\right)\right]xdx. \tag{4.19}$$

The derivation of the coverage probability in an open access method, which is given in A.6, is not as straightforward as closed access case due to the dependence of the user's SIR on r_1 and r_2. The derivations require evaluating a double integral which does not have a closed form. As a matter of fact, the number of integrals that needs to be evaluated is determined by the number of tiers in the network.

4.2.2. SFR Edge User

By using the similar approach in the previous section, the coverage probability of an edge user in a SFR system can found by

$$F_{SFR,op,edge}(k,T)=\frac{\pi\lambda_1\int_0^\infty e^{-\pi\lambda_1\upsilon(1+\rho(\frac{\eta_1}{\beta_1})+2\kappa\psi(\frac{\gamma}{\beta}T,\alpha))}dr_1dr_2}{\int_0^\infty\int_0^\infty 2\pi\lambda_1r_1 2\pi\lambda_2r_2e^{-\pi\lambda_1r_1^2}e^{-\pi\lambda_2r_2^2}g_d(r_1,r_2)dr_1dr_2}$$
$$\frac{-\int_0^\infty\int_0^\infty 2\pi\lambda_1r_1 2\pi\lambda_2r_2e^{-\pi\lambda_1r_1^2}e^{-\pi\lambda_2r_2^2}g_n(r_1,r_2)dr_1dr_2}{\int_0^\infty\int_0^\infty 2\pi\lambda_1r_1 2\pi\lambda_2r_2e^{-\pi\lambda_1r_1^2}e^{-\pi\lambda_2r_2^2}g_d(r_1,r_2)dr_1dr_2} \tag{4.20}$$

where

$$
\begin{aligned}
g_d(r_1, r_2) &= 1 - \epsilon_1 e^{-2\pi\lambda_1(\rho_{1,1}(\eta T_1,\alpha)+\kappa\rho_{1,2}(\gamma T_1,\alpha))} - \epsilon_2 e^{-2\pi\lambda_1(\rho_{2,1}(T_2/\gamma,\alpha)+\kappa\rho_{2,2}(T_2,\alpha))} \\
g_n(r_1, r_2) &= \epsilon_1 e^{-2\pi\lambda_1\left(\zeta_{1,1}(T,T_1,\alpha,\beta_1,\eta_1)+\kappa(\psi(\frac{\gamma}{\beta_1}T,\alpha)+\rho_{1,2}(\gamma T_1,\alpha))\right)} + \\
&\quad (\epsilon_2 - 1) e^{-2\pi\lambda_1\left(\zeta_{2,1}(T,T_2/\gamma,\alpha,\beta_1,\eta_1)+\kappa(\psi(\frac{\gamma\eta_2}{\beta_1}T,\alpha)+\rho_{2,2}(T_2,\alpha))\right)} \\
\zeta_{a,b}(y, z, \beta, \eta) &= \frac{1}{2(y-z)} \left(y\rho_{a,b}(y,\alpha) + z\rho_{a,b}(z,\alpha)\right) \\
\rho_{a,b}(z,\alpha) &= \int_{r_b}^{\infty} 1 - \frac{1}{1 + z r_a^{\alpha} x^{-\alpha}} x dx.
\end{aligned}
\tag{4.21}
$$

4.2.3. Simulation Results

The parameters employed in order to obtain MATLAB simulation results of a two-tier network system with open access scheme are summarized in Table 4.2.

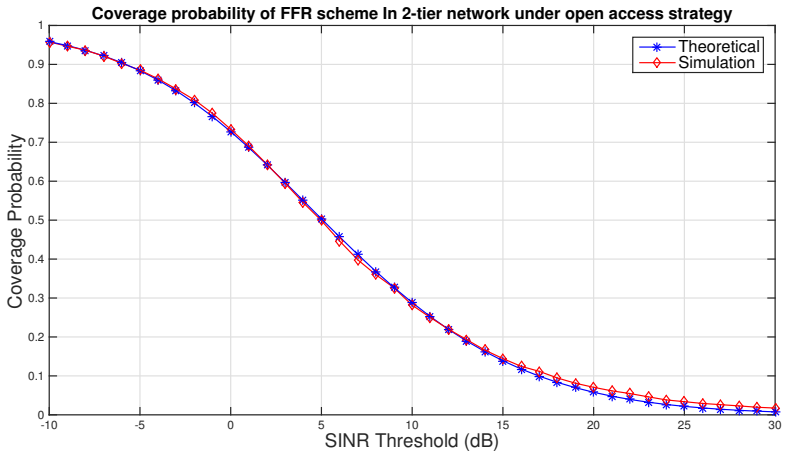

Figure 4.6. Coverage probability of strict FFR in a 2-tier network with $T_1 = 3$ dB, $T_2 = 5$ dB FFR threshold when there is no noise and $\alpha = 4$.

Figure 4.6 illustrates the simulation and theoretical results of the coverage probability of strict FFR in 2-tier network with $T_1 = 3$ dB, $T_2 = 5$ dB FFR threshold. This results suggest that our simulation results consistently match the theoretical analysis is shown in Section 4.2.1.

Table 4.2. Simulation parameters for a heterogeneous network with an open access policy.

Parameter	Value / Assumption
Cell geometry	Weighted Voronoi
BS distribution	PPP
Macro BS density (λ_1)	$1/4000\pi$ BSs/m^2
Femto BS density (λ_2)	$1/500\pi$ BSs/m^2
Density ratio (κ_{21})	8
Power ratio (γ_{21})	0.001
User distribution	PPP
User density (λ_u)	0.01 $users/m^2$
Edge user SINR threshold of macrocells	3 dB
Edge user SINR threshold of femtocells	5 dB
Pathloss exponent (α)	4
Number of total subbands	48
Reuse factor (Δ)	3
Frequency planning	Strict FFR SFR
Power control factor (β)	2,4,8,16 dB
Access scheme	Open Access

Figure 4.7 shows the comparison of coverage probabilities of strict FFR under closed and open access strategies, in which $T_1 = 5, T_2 = 1$ dB. As expected, open access performs better than closed access in terms of coverage probability.

Figure 4.8 depicts the comparison of coverage probability of SFR in 2-tier network for increasing β factors with $\kappa_{21} = 8, \gamma_{21} = 0.001, T_1 = 5, T_2 = 1$ dB. As β increases, coverage probability for edge users increases as well for a given SINR threshold. Figure 4.8 also provides a comparison of coverage probabilities for closed access and open

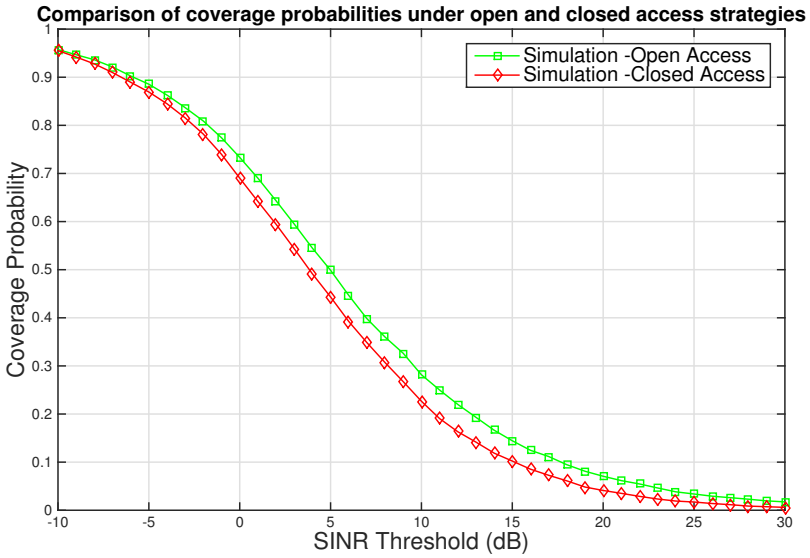

Figure 4.7. Comparison of coverage probabilities of FFR in 2-tier network under open and closed access with $T_1 = 3$ dB , $T_2 = 5$ dB FFR threshold when there is no noise and $\alpha = 4$.

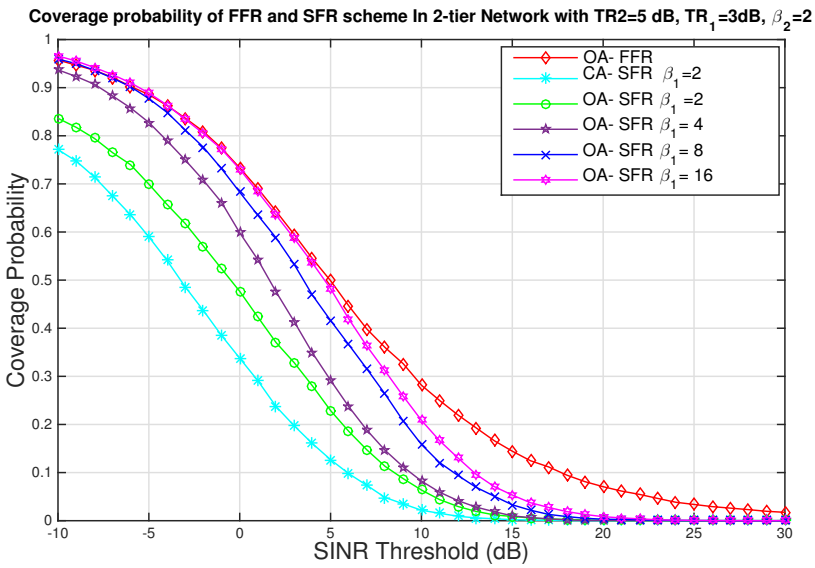

Figure 4.8. Coverage probability of SFR in 2-tier network of macrocells and femtocells with $\kappa_{21} = 8, \gamma_{21} = 0.001, T_1 = 5, T_2 = 1$ dB when there is no noise and $\alpha = 4$.

access strategies under SFR scheme, in which $\beta = 2$. It is worth noting that using an open access assignment, instead of a closed access scheme, provides approximately 3 dB improvement for the same level of coverage probability under SFR, which is higher improvement than the case in strict FFR. It is a quite reasonable result since there is

cross-tier interference in SFR, whereas there is cross-tier interference removal and $1/\Delta$ thinning of the intra-tier interference as demonstrated in Figure 4.1. Hence, better assignment strategy results in more improvement in the interference for the case of SFR compared to strict FFR.

4.3. Conclusion

When node and user distributions follow a PPP distribution, the simulated results consistently match the theoretical analysis for both strict FFR and SFR techniques in a multi-tier network as seen in Figure 4.3, Figure 4.5,Figure 4.6, Figure 4.8. Effect of mobility will be investigated in the next chapter.

5. MOBILITY EVALUATION OF CELLULAR NETWORKS

In this chapter, mobility evaluation of cellular networks will be discussed by providing different approaches to handling mobility. We propose three different perspectives on mobility: Poisson line process (PLP) as a population model, basic uniform mobility model with random angle and fixed velocity and random way point (RWP) based mobility. PLP model is considered for the city topologies that contain main roads or routes. Second method is used to represent user mobility in a linear direction with a random angle θ. Third approach exploits RWP model to consider fluctuations in the channel gains as an another type of fading, in addition to multipath fading, which is caused due to change in the distance and path loss.

For practical purposes, it is assumed that the nodes are highly mobile, therefore, different time slots have independent realizations of node places. Channels are also considered as memoryless so that the node movements are not influenced by prior movements. It is important to observe that assumption of i.i.d. for user distribution in different time slots can be meaningful only if entirely new realizations of the user placement is obtained in each time slot [54]. Since the users do not possess infinite mobility, the user locations in different time slots are correlated in practice. Nevertheless, we presume that the transmission begins at the beginning of each time slot, and each transmission is completed within one time slot for the sake of simplicity and we investigate the performance of the network in a single snapshot.

5.1. Poison Line Process (PLP)

The model in which users are distributed to the topology of the cities which includes roads can be described by a Cox process driven by a Poisson line tessellation. In our model, roads are distributed on a map according to a Poisson line process, while users on each road are distributed independently according to stationary Poisson point

processes. Manhattan city model can be considered as a special case of this generalized random model.

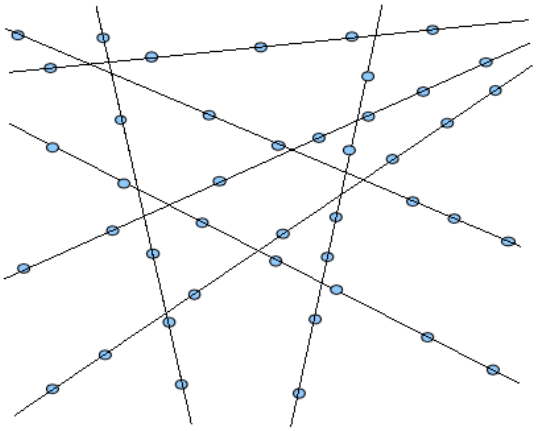

Figure 5.1. Random nodes on random lines [4].

Let D is a line on $\mathbb{R}^2$ and (θ, r) represents the polar coordinates of the orthogonal projection of the origin O on D, which can be described by $d : (\theta, r) \mapsto D$. For $\theta \in [0; \pi)$ and $r \in \mathbb{R}$, (θ, r) uniquely designates the polar coordinates. Then, a Poisson line process with intensity λ is the image by d, of a PPP Φ with an intensity λ on half-cylinder $[0; \pi) \times \mathbb{R}$.

For $\mu > 0$, Φ can be associated with a random measure Λ that is the total length of roads intersecting a given area can be computed by

$$\forall A \subset \mathbb{R}^2, \Lambda(A) = \sum_{(\theta,r)\in\Phi} \mu l(A \cap d(\theta, r)), \tag{5.1}$$

where l is the 1-dimensional Lebesgue measure, as in [50]. Hence the population process can be modeled by a Cox process with underlying measure Λ. As proved in [38], under Palm distribution, Φ, Poisson point process with intensity Λ, is stationary and isotropic with intensity $\pi\lambda\mu$ and it is the sum stationary Φ of an independent μ-Poisson point process on a line through O with an independent uniform angle, and of an atom at O. This theorem helps us to divide the Laplace functional into two parts in the following derivations.

Let $f : \mathbb{R}^d \to \mathbb{R}^+$ and if f has a radial symmetry, i.e. $f(x) = f(\|x\|)$, the Laplace functional of PLP is computed in [38] by

$$\mathcal{L}_\Phi(f) = exp\left[-2\pi\lambda \int_{u\geq 0} \left(1 - exp(-2\mu \int_{t\geq 0} \left(1 - e^{-f(\sqrt{u^2+t^2})} dt\right)\right) du\right]. \tag{5.2}$$

For the scenario, where there is no an ICIC technique such as strict FFR or SFR and there is only one type of base station, the coverage probability of uplink is derived in [38]. By using similar approach, the coverage probability of downlink network system can be derived as

$$p_{cov,plp}(T, \lambda, \alpha, r) = \pi\lambda_a \int_0^\infty e^{-\pi\lambda_a r^2} e^{-\mu T\sigma^2 r^\alpha} \mathcal{L}_{I_p}(Tr^\alpha) r dr, \tag{5.3}$$

where

$$\begin{aligned}
\mathcal{L}_{I_p} &= m(T, r)n(T, r) \\
m(T, r) &= exp\left(-2\pi\lambda r \int_0^\infty \left(1 - exp\left(-2\mu r \int_0^\infty 1 \frac{1}{1 + \frac{(u^2+t^2)^{\alpha/2}}{T}} dt\right)\right) dr\right) \\
n(T, r) &= \frac{1}{\pi} \int_0^\infty exp\left(-2\mu r \int_0^\infty 1 \frac{1}{1 + \frac{(sin^2\theta+t^2)^{\alpha/2}}{T}} dt\right) d\theta.
\end{aligned} \tag{5.4}$$

Figure 5.2 demonstrates that modeling users with PLP + PPP simulations give slightly higher coverage probability in a single tier network which is composed of macrocells only. Figure 5.3 depicts that under closed access strategy, coverage probability of a two-tier network of macrocells and femtocells decreases when PLP and PPP models are used together to model the user distribution, whereas figure 5.4 illustrates the performance of coverage probability under open access. We can observe that if femtocells are also distributed on a Poisson line route, coverage probability again reaches the limits of PPP model. As a result, we may conclude that it is crucial to take the PLP effect into account to guarantee certain level of QoS in a heterogeneous network while designing the network topology.

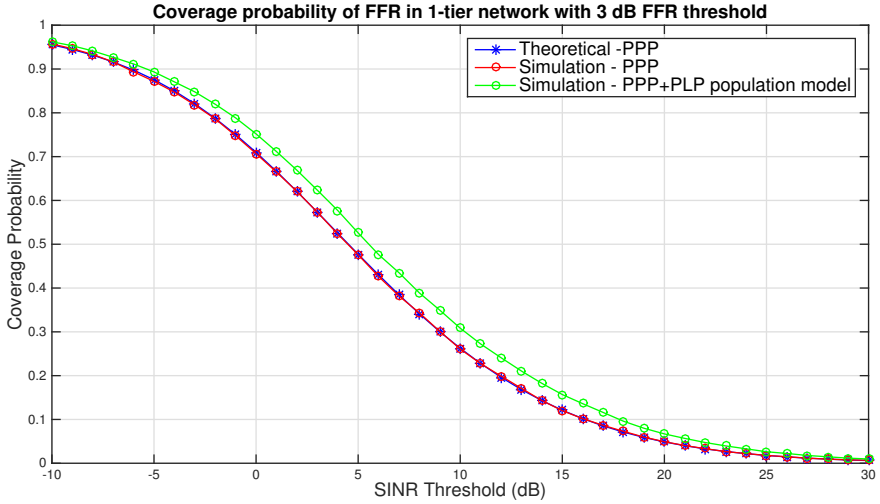

Figure 5.2. Coverage probability of FFR in 1-tier network with 3 dB FFR threshold when there is no noise and $\alpha = 4$.

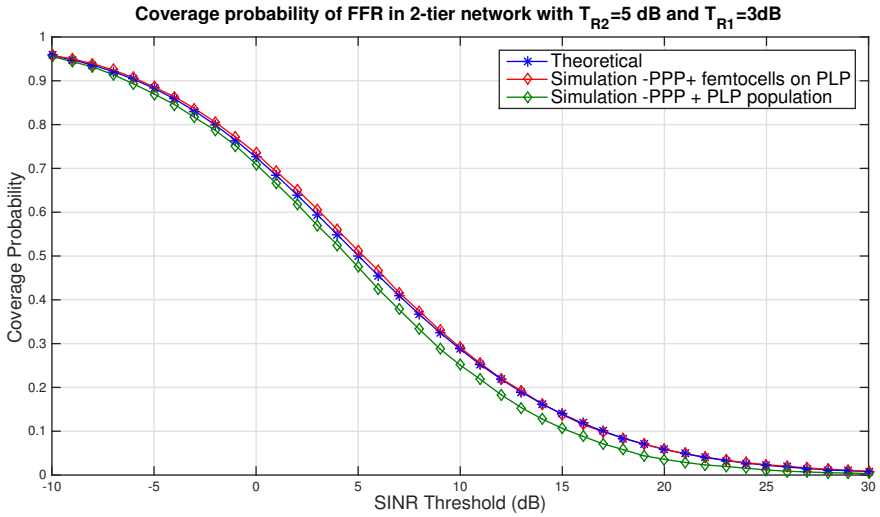

Figure 5.3. Coverage probability of FFR in 2-tier network under closed access strategy with $T_1 = 3$ dB, $T_2 = 5$ dB FFR threshold when there is no noise and $\alpha = 4$.

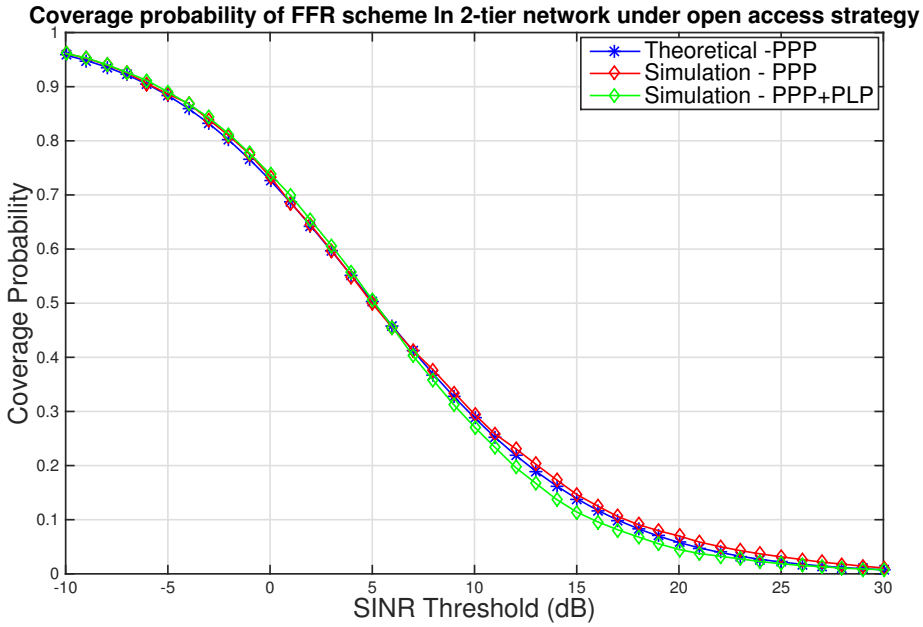

Figure 5.4. Coverage probability of strict FFR in 2-tier network under open access with $T_1 = 3$ dB , $T_2 = 5$ dB FFR threshold when there is no noise and $\alpha = 4$.

5.2. User mobility in a linear direction with a random angle θ

Assume that the user moves with the average velocity $\bar{v}$ for a given duration Δt, the moving user is served by a macro BS if SINR of the moving user is greater than or equal to a given SINR threshold T during the period Δt. r_p represents the distance between serving macro BS and initial point of moving user, while $\Delta r = \bar{v}\Delta t$ represents the change in the distance due to the movement of the user. Thus, the function of distance between serving macro BS and the location of moving user can be calculated as $r_m = \sqrt{r_p^2 + \Delta r^2 - 2r_p\Delta r cos\theta}$, where θ denotes the angle between movement direction of the user and distance vector of r_p.

5.2.1. When user moves with θ in a single tier network

When there is not any ICIC technique that is employed, general framework for calculation of coverage probability is given by

$$\begin{aligned}
p_c(T,\lambda,\alpha) &= \mathbb{P}[SINR > T] \\
&= \mathbb{P}\left[\frac{hr^{-\alpha}}{\sigma^2 + I_r} > T\right] \\
&= \mathbb{P}\left[\frac{hr^{-\alpha}}{\sigma^2 + \sum_{i\in\Phi/b_o} g_i R_i^{-\alpha}} > T\right] \\
&= \mathbb{E}_r[\mathbb{P}[SINR > T|r]] \\
&= \int_{r>0} \mathbb{P}[SINR > T|r] f_r(r) dr \\
&= \int_{r>0} \mathbb{P}[h > Tr^{\alpha}(\sigma^2 + I_r)|r] f_r(r) dr \\
&= \int_{r>0} \mathbb{E}_{I_r}[e^{-\mu T r^{\alpha}(\sigma^2 + I_r)}|r] f_r(r) dr \\
&= \int_{r>0} e^{-\mu T r^{\alpha}\frac{\sigma^2}{P}} \mathcal{L}_{I_r}(\mu T r^{\alpha}) f_r(r) dr. \qquad (5.5)
\end{aligned}$$

In the previous cases in which there is no mobility, pdf of r was found out as $f_r(r) = 2\pi\lambda r e^{-\lambda\pi r^2}$. If we update the pdf of r accordingly, we obtain

$$\begin{aligned}
f_{r_m}(r) &= \frac{d\mathbb{P}\left(\sqrt{r_p^2 + \Delta r^2 - 2r_p\Delta r\cos\theta} < r\right)}{dr} \\
&= \frac{d\left(\frac{1}{\pi}\int_0^{\pi}\int_0^{\Delta r cos\theta + \sqrt{r^2 + (\Delta r\cos\theta)^2 - \Delta r^2}} 2\pi\lambda y e^{-\pi\lambda y^2} dy\right)}{dr} \\
&= \frac{1}{\pi}\int_0^{\pi} \frac{2\pi x\lambda w(r,\theta) e^{-\pi\lambda(w(r,\theta))^2}}{w(r,\theta) - \Delta r\cos\theta} d\theta \qquad (5.6)
\end{aligned}$$

where $w(r,\theta) = \Delta r\cos\theta + \sqrt{r^2 + (\Delta r\cos\theta)^2 - \Delta r^2}$.

When $g_i \sim exp(\mu)$, i.e. distribution of interference is Rayleigh too, $\mathcal{L}_{I_r}(\mu T r^{\alpha})$ becomes

$$\mathcal{L}_{I_r}(\mu T r^{\alpha}) = exp(-\pi r^2 \lambda \rho(T, \alpha)). \tag{5.7}$$

If there is not any noise, equation (5.5) turns into

$$p_c(T, \lambda, 4, \theta) = \int_0^{\infty} e^{-\pi r^2 \lambda \rho(T,4)} \left(\frac{1}{\pi} \int_0^{\pi} \frac{2\pi x \lambda w(r,\theta) e^{-\pi \lambda (w(r,\theta))^2}}{w(r,\theta) - \Delta r \cos\theta} d\theta \right) dr. \tag{5.8}$$

FFR - 1 Tier Network Case.

By inserting (4.6) and (5.6) into (5.5), we get

$$p_c(T, T_{FR}, \lambda, 4, \theta, \Delta) = \int_0^{\infty} e^{-2\pi r^2 \lambda \xi(T, T_{FR}, 4, \Delta)} e^{-\mu(T+T_{FR}) r^{\alpha} \frac{\sigma^2}{P}} \times \left(\frac{1}{\pi} \int_0^{\pi} \frac{2\pi x \lambda w(r,\theta) e^{-\pi \lambda (w(r,\theta))^2}}{w(r,\theta) - \Delta r \cos\theta} d\theta \right) dr. \tag{5.9}$$

Simulation result for this case is shown in Figure 5.5(a). Snapshot analysis for different time realizations gives the same simulation result for static case under this mobility model.

SFR - 1 Tier Network Case.

By inserting (3.15) and (5.6) into (5.5), we get

$$p_c(T, T_{FR}, \lambda, 4, \theta, \beta, \eta) = \int_0^{\infty} e^{-2\pi r^2 \lambda \zeta(T, T_{FR}, \alpha, 1, \eta, \beta)} e^{-\mu(T+T_{FR}) r^{\alpha} \frac{\sigma^2}{P}} \times \left(\frac{1}{\pi} \int_0^{\pi} \frac{2\pi x \lambda w(r,\theta) e^{-\pi \lambda (w(r,\theta))^2}}{w(r,\theta) - \Delta r cos\theta} d\theta \right) dr. \tag{5.10}$$

Simulation result for this case is shown in Figure 5.5(b). Snapshot analysis for different time realizations gives the same simulation result for static case under this mobility model.

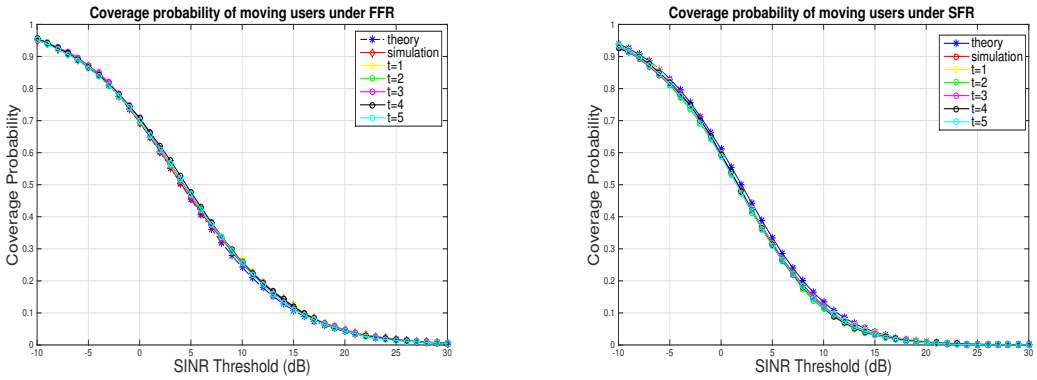

(a) Strict FFR case. (b) SFR case.

Figure 5.5. Coverage probability in 1-tier network with 3 dB FFR threshold when user moves with θ and there is no noise, $\alpha = 4$.

5.2.2. When user moves with θ in a two-tier network

Figure 5.6(a) and Figure 5.6(b) provide the simulation results of coverage probabilities in a 2-tier network under the given mobility model for strict FFR and SFR cases, respectively. Similarly, we obtain the same simulation results for different time realizations as in the static case under this mobility model.

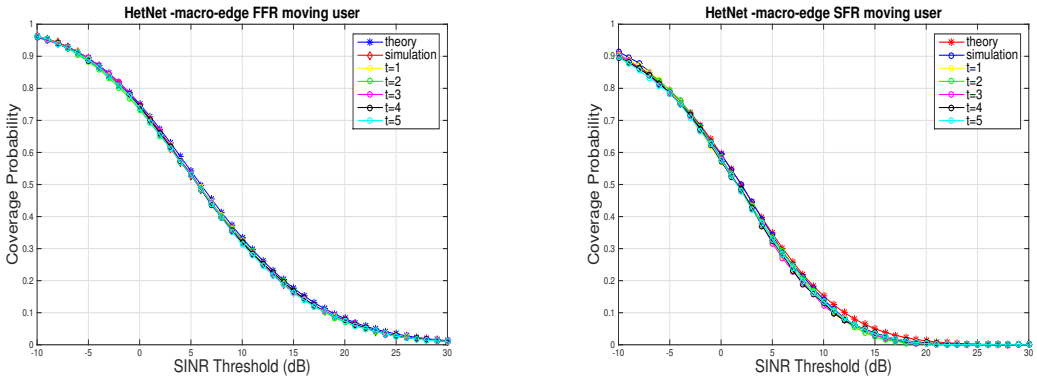

(a) Strict FFR case. (b) SFR case.

Figure 5.6. Coverage probability of macrocell in a 2-tier network with 3 dB FFR threshold when users move randomly and independently in the case where there is no noise and $\alpha = 4$.

5.2.3. When femtocell moves with θ in a two-tier network

We have also investigated the case in which femtocell moves with its subscribed users along the linear path under closed access scheme. Figure 5.7(a) and Figure 5.7(b) provide the simulation results of coverage probabilities of macrocell-tier users under the given mobility model for strict FFR and SFR cases, respectively.

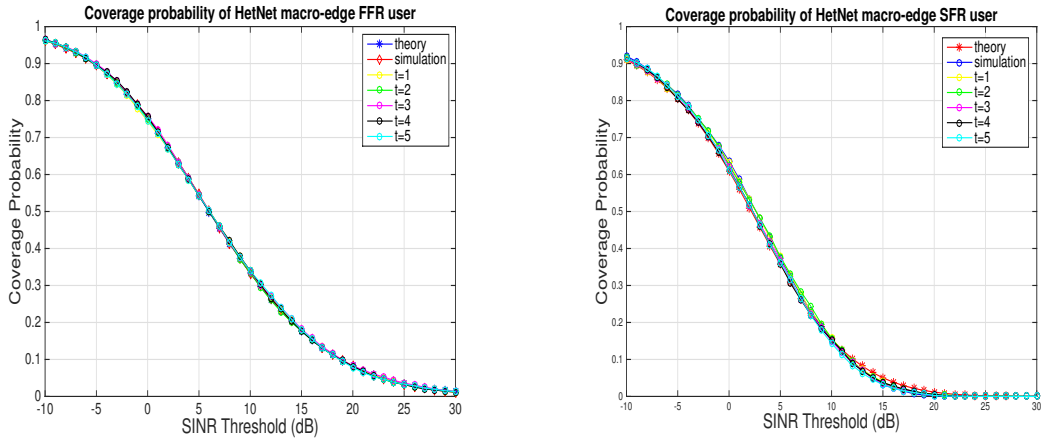

(a) Strict FFR case. (b) SFR case.

Figure 5.7. Coverage probability of macrocell in a 2-tier network with 3 dB FFR threshold when femtocells move randomly and independently in the case where there is no noise and $\alpha = 4$.

5.2.4. Conclusion

Outlined results supports the idea that the snapshot analysis of cellular networks in any given time can be considered as a correlated realization of a static network as a consequence of the uniformity of the mobility. Therefore, the previous derivations of the interference and coverage probability in static networks are also valid for the case of uniformly mobile networks [48].

5.3. Mobility as a Fading Model

Changes in distance, hence the path loss, between the user and access points which are induced by the mobility cause fluctuations in the channel gains. [54] has shown that fluctuations might be considered as another type of fading in addition to multipath fading. Fading can be grouped into two categories: multipath fading which is generated by microscopic mobility and large-scale fading which is induced by significant variation in the transmission distance, i.e. macroscopic mobility.

In our analysis, we consider random waypoint (RWP) mobility model which takes pause times between random changes in direction and speed into account. We derive the coverage probability of macrocell edge users under strict FFR scheme for this mobility approach. By following the directions that are presented in the previous chapters, it can be extended to SFR scheme and heterogeneous network case in the similar manner.

In [55], the probability density function of the distance of a typical node to the origin for RWP mobility model in $B(o, R)$ is given as

$$f_L(r) = \frac{1}{R^2}\left(-\frac{4r^3}{R^2} + 4r\right). \tag{5.11}$$

Thus, density measure of the p.p. can be found by

$$\Lambda(B(o, R)) \triangleq \mathbb{E}\left[\Phi(B(o, R))\right] = 2\lambda\pi r^2 - \frac{\lambda\pi r^4}{R^2} \tag{5.12}$$

where $r \leqslant R$. Hence, the radial density function becomes

$$\lambda(r) = 4\lambda\pi r - \frac{4\lambda\pi r^3}{R^2}. \tag{5.13}$$

Conditioning on the total number of nodes M, we get

$$\begin{aligned}\mathbb{P}\left(R_1 \leq r|M\right) &= 1-\left(1-F_L(r)\right)^M \\ &= 1-\left(1-\left(\frac{2r^2}{R^2}-\frac{r^4}{R^4}\right)\right)^M. \end{aligned} \tag{5.14}$$

As M has a Poisson distribution with mean $\lambda\pi R^2$, the pdf of R_1 is calculated as

$$\begin{aligned} f_{R_1}(r) &= \frac{d\mathbb{E}_M\left[\mathbb{P}\left(R_1 \leq r|M\right)\right]}{dr} \\ &= \lambda\pi\left(4r-\frac{4r^3}{R^2}\right)e^{-\lambda\pi\left(2r^2-\frac{r^4}{R^2}\right)}. \end{aligned} \tag{5.15}$$

It is shown in [48] that taking the interference from the closest interferer into account gives a good approximation because of decrease in the received power as a result of the power law, when the path-loss exponent α is not very close to 2, . Hence, the interference power can be approximated by $I \approx I_1 = R^{-\alpha}$, where R_1 is the distance between the user and its closest interferer. Thus,

$$f_{I_1}(x) = \lambda\pi\frac{4}{\alpha}\left(x^{-2/\alpha-1}-\frac{x^{-4/\alpha-1}}{R^2}\right)e^{-\lambda\pi\left(2x^{-2/\alpha}-\frac{x^{-4/\alpha}}{R^2}\right)} \tag{5.16}$$

and

$$F_{I_1}(x) = e^{-\lambda\pi\left(2x^{-2/\alpha}-\frac{x^{-4/\alpha}}{R^2}\right)}. \tag{5.17}$$

Considering the interference-limited network, when there is multipath fading and the interference power from the nearest interferer is $g_1 I_1$, coverage probability of cell-edge users under strict FFR can be calculated by

$$
\begin{aligned}
F_{FFR}(T) &= \mathbb{P}\left(\frac{\hat{g}}{\hat{g_1}\hat{I_1}} > T \middle| \frac{g}{g_1 I_1} < T_{FR}\right) \\
&= \frac{\mathbb{P}\left(\frac{\hat{g}}{\hat{g_1}\hat{I_1}} > T, \frac{g}{g_1 I_1} < T_{FR}\right)}{\mathbb{P}\left(\frac{g}{g_1 I_1} < T_{FR}\right)} \\
&= \frac{\mathbb{P}\left(\frac{\hat{H}}{T} > \hat{I_1}, \frac{H}{T_{FR}} < I_1\right)}{\mathbb{P}\left(\frac{H}{T_{FR}} < I_1\right)} \\
&= \frac{\mathbb{E}\left[\mathbb{P}\left(\frac{\hat{H}}{T} > \hat{I_1}, \frac{H}{T_{FR}} < I_1\right)\right]}{\mathbb{E}\left[\mathbb{P}\left(\frac{H}{T_{FR}} < I_1\right)\right]}
\end{aligned}
\tag{5.18}
$$

where $H = g/g_1$. Assuming that there is Rayleigh fading, pdf of H is found as

$$
f_H(x) = \frac{1}{(x+1)^2}. \tag{5.19}
$$

Hence, (5.18) becomes

$$
\begin{aligned}
F_{FFR}(T) = &\frac{\int_0^\infty \left(exp\left(-\lambda\pi(2T^{2/\alpha}x^{-2/\alpha} - \frac{T^{4/\alpha}x^{-4/\alpha}}{R^2})\right)\right)\frac{1}{(x+1)^2}dx}{1 - \int_0^\infty exp\left(-\lambda\pi(2T_{FR}^{2/\alpha}x^{-2/\alpha} - \frac{T_{FR}^{4/\alpha}x^{-4/\alpha}}{R^2})\right)\frac{1}{(x+1)^2}dx} - \\
&\frac{\int_0^\infty \left(exp\left(-\lambda\pi(2x^{-2/\alpha}(T^{2/\alpha} + T_{FR}^{2/\alpha}) - \frac{x^{-4/\alpha}(T^{4/\alpha}+T_{FR}^{4/\alpha})}{R^2})\right)\right)\frac{1}{(x+1)^2}dx}{1 - \int_0^\infty exp\left(-\lambda\pi(2T_{FR}^{2/\alpha}x^{-2/\alpha} - \frac{T_{FR}^{4/\alpha}x^{-4/\alpha}}{R^2})\right)\frac{1}{(x+1)^2}dx}.
\end{aligned}
\tag{5.20}
$$

Authors in [45], have shown that SIR distributions of different cellular network models can be approximated by a certain horizontal shift of the distribution of PPP model by considering mean interference-to-signal ratio between the network model and PPP model. Figure 5.8 depicts the required horizontal shift between the analysis and

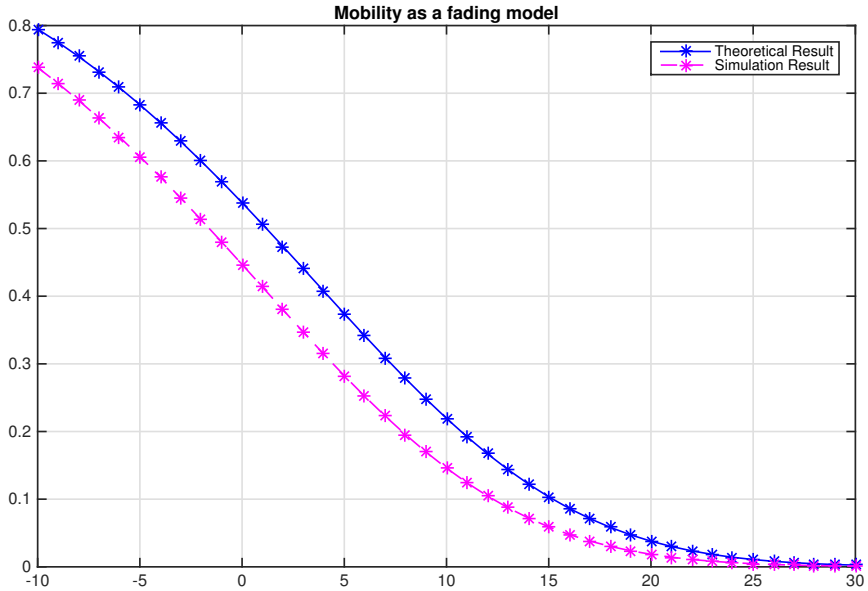

Figure 5.8. Coverage probability of macrocell edge users under strict FFR scheme when mobility is treated as a fading.

simulation results of coverage probabilities for the case of in single-tier network under strict FFR scheme. This approach can be also used to find the coverage probabilities in heterogeneous networks when mobility becomes an issue to be handled.

6. CONCLUSION

In this thesis, mathematical modeling of PPP-based network model and analysis of the network performance are investigated by using stochastic geometry tools. In Chapter 2, we have introduced the necessary properties of stochastic geometry in order to obtain performance evaluation of single tier and multi-tier networks in terms of SINR and coverage probability in Chapter 3 and Chapter 4 respectively, under strict FFR and SFR schemes. Since small cells are becoming an essential part of future LTE networks, we have proposed methods to examine the impact of user mobility on heterogeneous networks in Chapter 5.

We have used mainly SINR and the coverage probability as a network performance metrics. However, this can be extended to evaluation of average ergodic data rate assuming that users can achieve Shannon bound by using their instantaneous SINR, i.e. $\mathbb{E}\left[ln(1+SINR)\right]$.

We modeled the network by using PPP throughout the thesis. Nevertheless, it is better to introduce Poisson cluster process (PCP) to model the network when the nodes are clustered around highly populated regions in the future work.

Modern cellular systems consist of multi-tiers of BSs with dense base station deployments in order to enhance the network performance in terms of the coverage probability and network capacity. There is a huge opportunity to improve the performance metrics by introducing effective offloading algorithms with the integration of small cells. Therefore, including handover and offloading algorithms by using stochastic geometry is a further challenge that needs to be addressed when both the femtocells and users are moving as a future research direction.

REFERENCES

1. Zhang, J. and G. de la Roche, *Femtocells: Technologies and Deployment*, Wiley Publishing, 2010.

2. Gok, A. and M. Koca, "Performance evaluation of frequency planning and scheduling schemes in OFDMA Networks", *2014 IEEE International Black Sea Conference on Communications and Networking (BlackSeaCom)*, pp. 149–153, May 2014.

3. Novlan, T. D., R. K. Ganti, A. Ghosh and J. G. Andrews, "Analytical Evaluation of Fractional Frequency Reuse for Heterogeneous Cellular Networks", *IEEE Transactions on Communications*, Vol. 60, No. 7, pp. 2029–2039, July 2012.

4. Błaszczyszyn, B. and P. Mühlethaler, "Random Linear Multihop Relaying in a General Field of Interferers Using Spatial Aloha", *IEEE Transactions on Wireless Communications*, Vol. 14, No. 7, pp. 3700–3714, July 2015.

5. Zyren, J., "White Paper Overview of the 3GPP Long Term Evolution Physical Layer", Online, July 2007, `http://www.nxp.com/assets/documents/data/en/white-papers/3GPPEVOLUTIONWP.pdf`, accessed at December 2016.

6. 3GPP, *TS 36.133 version 9.3.0 Release 9*, Tech. rep., April 2010.

7. Alouini, M. S. and A. J. Goldsmith, "Area spectral efficiency of cellular mobile radio systems", *IEEE Transactions on Vehicular Technology*, Vol. 48, No. 4, pp. 1047–1066, July 1999.

8. Chandrasekhar, V., J. G. Andrews and A. Gatherer, "Femtocell networks: a survey", *IEEE Communications Magazine*, Vol. 46, No. 9, pp. 59–67, September 2008.

9. Kendall, W. and I. Molchanov, *New Perspectives in Stochastic Geometry*, OUP Oxford, 2009.

10. Hamza, A. S., S. S. Khalifa, H. S. Hamza and K. Elsayed, "A Survey on Inter-Cell Interference Coordination Techniques in OFDMA-Based Cellular Networks", *IEEE Communications Surveys Tutorials*, Vol. 15, No. 4, pp. 1642–1670, April 2013.

11. Cullen, J., "Radioframe presentation", *Femtocell Europe 2008, London, UK*, June 2008.

12. Andrews, J. G., S. Buzzi, W. Choi, S. V. Hanly, A. Lozano, A. C. K. Soong and J. C. Zhang, "What Will 5G Be?", *IEEE Journal on Selected Areas in Communications*, Vol. 32, No. 6, pp. 1065–1082, June 2014.

13. Fleming, P. J., B. Simon and A. Stolyar, *Closed-Form Expressions for Other-Cell Interference in Cellular CDMA*, Tech. rep., Denver, CO, USA, 1997.

14. Baccelli, F., M. Klein, M. Lebourges and S. Zuyev, "Stochastic geometry and architecture of communication networks", *Telecommunication Systems*, Vol. 7, No. 1, pp. 209–227, 1997.

15. Gupta, P. and P. R. Kumar, "The capacity of wireless networks", *IEEE Transactions on Information Theory*, Vol. 46, No. 2, pp. 388–404, Machr 2000.

16. Weber, S. P., X. Yang, J. G. Andrews and G. de Veciana, "Transmission capacity of wireless ad hoc networks with outage constraints", *IEEE Transactions on Information Theory*, Vol. 51, No. 12, pp. 4091–4102, December 2005.

17. Baccelli, F., B. Blaszczyszyn and P. Muhlethaler, "An Aloha protocol for multihop mobile wireless networks", *IEEE Transactions on Information Theory*, Vol. 52, No. 2, pp. 421–436, February 2006.

18. Baccelli, F. and B. Blaszczyszyn, "A new phase transitions for local delays in MANETs", *2010 Proceedings IEEE INFOCOM*, pp. 1–9, March 2010.

19. Hanawal, M. K., E. Altman and F. Baccelli, "Stochastic Geometry Based Medium

Access Games in Wireless Ad Hoc Networks", *IEEE Journal on Selected Areas in Communications*, Vol. 30, No. 11, pp. 2146–2157, December 2012.

20. Haenggi, M., *Stochastic Geometry for Wireless Networks*, Cambridge University Press, 2012.

21. Andrews, J. G., F. Baccelli and R. K. Ganti, "A Tractable Approach to Coverage and Rate in Cellular Networks", *IEEE Transactions on Communications*, Vol. 59, No. 11, pp. 3122–3134, November 2011.

22. Wu, L., Y. Zhong and W. Zhang, "Spatial Statistical Modeling for Heterogeneous Cellular Networks - An Empirical Study", *2014 IEEE 79th Vehicular Technology Conference (VTC Spring)*, pp. 1–6, May 2014.

23. Novlan, T. D., R. K. Ganti, A. Ghosh and J. G. Andrews, "Analytical Evaluation of Fractional Frequency Reuse for OFDMA Cellular Networks", *IEEE Transactions on Wireless Communications*, Vol. 10, No. 12, pp. 4294–4305, December 2011.

24. Zhang, X. and M. Haenggi, "A Stochastic Geometry Analysis of Inter-Cell Interference Coordination and Intra-Cell Diversity", *IEEE Transactions on Wireless Communications*, Vol. 13, No. 12, pp. 6655–6669, December 2014.

25. De La Roche, G., A. Valcarce, D. Lopez-Perez and J. Zhang, "Access control mechanisms for femtocells", *IEEE Communications Magazine*, Vol. 48, No. 1, pp. 33–39, January 2010.

26. Jo, H.-S., P. Xia and J. G. Andrews, "Open, closed, and shared access femtocells in the downlink", *EURASIP Journal on Wireless Communications and Networking*, Vol. 2012, No. 1, pp. 1–16, 2012.

27. Shafigh, A. S., P. Mertikopoulos and S. Glisic, "A novel dynamic network architecture model based on stochastic geometry and game theory", *2016 IEEE International Conference on Communications (ICC)*, pp. 1–7, May 2016.

28. Arshad, R., H. ElSawy, S. Sorour, T. Y. Al-Naffouri and M. S. Alouini, "Handover management in dense cellular networks: A stochastic geometry approach", *2016 IEEE International Conference on Communications (ICC)*, pp. 1–7, May 2016.

29. Sadr, S. and R. S. Adve, "Handoff Rate and Coverage Analysis in Multi-Tier Heterogeneous Networks", *IEEE Transactions on Wireless Communications*, Vol. 14, No. 5, pp. 2626–2638, May 2015.

30. Bandyopadhyay, S., E. J. Coyle and T. Falck, "Stochastic Properties of Mobility Models in Mobile Ad Hoc Networks", *IEEE Transactions on Mobile Computing*, Vol. 6, No. 11, pp. 1218–1229, November 2007.

31. Bettstetter, C., G. Resta and P. Santi, "The node distribution of the random waypoint mobility model for wireless ad hoc networks", *IEEE Transactions on Mobile Computing*, Vol. 2, No. 3, pp. 257–269, July 2003.

32. Hyytia, E., P. Lassila and J. Virtamo, "Spatial node distribution of the random waypoint mobility model with applications", *IEEE Transactions on Mobile Computing*, Vol. 5, No. 6, pp. 680–694, June 2006.

33. Lin, X., R. K. Ganti, P. J. Fleming and J. G. Andrews, "Fundamentals of mobility in cellular networks: Modeling and analysis", *2012 IEEE Global Communications Conference (GLOBECOM)*, pp. 5433–5438, December 2012.

34. Gong, Z. and M. Haenggi, "Mobility and Fading: Two Sides of the Same Coin", *2010 IEEE Global Telecommunications Conference (GLOBECOM 2010)*, pp. 1–5, December 2010.

35. Ganti, R. K. and M. Haenggi, "Interference and Outage in Clustered Wireless Ad Hoc Networks", *IEEE Transactions on Information Theory*, Vol. 55, No. 9, pp. 4067–4086, September 2009.

36. Saha, C. and H. S. Dhillon, "Downlink coverage probability of K-tier HetNets with

general non-uniform user distributions", *2016 IEEE International Conference on Communications (ICC)*, pp. 1–6, May 2016.

37. Chun, Y. J., M. O. Hasna and A. Ghrayeb, "Modeling Heterogeneous Cellular Networks Interference Using Poisson Cluster Processes", *IEEE Journal on Selected Areas in Communications*, Vol. 33, No. 10, pp. 2182–2195, October 2015.

38. Morlot, F., "A population model based on a Poisson line tessellation", *2012 10th International Symposium on Modeling and Optimization in Mobile, Ad Hoc and Wireless Networks (WiOpt)*, pp. 337–342, May 2012.

39. Schilcher, U., S. Toumpis, M. Haenggi, A. Crismani, G. Brandner and C. Bettstetter, "Interference Functionals in Poisson Networks", *IEEE Transactions on Information Theory*, Vol. 62, No. 1, pp. 370–383, January 2016.

40. Novlan, T. D., H. S. Dhillon and J. G. Andrews, "Analytical Modeling of Uplink Cellular Networks", *IEEE Transactions on Wireless Communications*, Vol. 12, No. 6, pp. 2669–2679, June 2013.

41. Dhillon, H. S., M. Kountouris and J. G. Andrews, "Downlink coverage probability in MIMO HetNets", *2012 Conference Record of the Forty Sixth Asilomar Conference on Signals, Systems and Computers (ASILOMAR)*, pp. 683–687, November 2012.

42. Gupta, A. K., H. S. Dhillon, S. Vishwanath and J. G. Andrews, "Downlink coverage probability in MIMO HetNets with flexible cell selection", *2014 IEEE Global Communications Conference*, pp. 1534–1539, December 2014.

43. Afify, L. H., H. ElSawy, T. Y. Al-Naffouri and M. S. Alouini, "Unified tractable model for downlink MIMO cellular networks using stochastic geometry", *2016 IEEE International Conference on Communications (ICC)*, pp. 1–7, May 2016.

44. Jo, H. S., Y. J. Sang, P. Xia and J. G. Andrews, "Heterogeneous Cellular Networks

with Flexible Cell Association: A Comprehensive Downlink SINR Analysis", *IEEE Transactions on Wireless Communications*, Vol. 11, No. 10, pp. 3484–3495, October 2012.

45. Ganti, R. K. and M. Haenggi, "Asymptotics and Approximation of the SIR Distribution in General Cellular Networks", *IEEE Transactions on Wireless Communications*, Vol. 15, No. 3, pp. 2130–2143, March 2016.

46. Wei, H., N. Deng, W. Zhou and M. Haenggi, "Approximate SIR Analysis in General Heterogeneous Cellular Networks", *IEEE Transactions on Communications*, Vol. 64, No. 3, pp. 1259–1273, March 2016.

47. Renzo, M. D., W. Lu and P. Guan, "The Intensity Matching Approach: A Tractable Stochastic Geometry Approximation to System-Level Analysis of Cellular Networks", *IEEE Transactions on Wireless Communications*, Vol. 15, No. 9, pp. 5963–5983, September 2016.

48. Haenggi, M. and R. K. Ganti, "Interference in Large Wireless Networks", *Foundations and Trends in Networking*, Vol. 3, No. 2, pp. 127–248, 2009.

49. Mukherjee, S., *Analytical Modeling of Heterogeneous Cellular Networks*, Cambridge University Press, 2014.

50. Chiu, S., D. Stoyan, W. Kendall and J. Mecke, *Stochastic Geometry and Its Applications*, Wiley Series in Probability and Statistics, Wiley, 2013.

51. Baccelli, F. and B. Błaszczyszyn, "Stochastic Geometry and Wireless Networks: Volume I Theory", *Foundations and Trends in Networking*, Vol. 3, No. 3–4, pp. 249–449, 2010.

52. Novlan, T., J. G. Andrews, I. Sohn, R. K. Ganti and A. Ghosh, "Comparison of Fractional Frequency Reuse Approaches in the OFDMA Cellular Downlink", *Global Telecommunications Conference (GLOBECOM 2010), 2010 IEEE*, pp. 1–

5, December 2010.

53. ElSawy, H., E. Hossain and M. Haenggi, "Stochastic Geometry for Modeling, Analysis, and Design of Multi-Tier and Cognitive Cellular Wireless Networks: A Survey", *IEEE Communications Surveys Tutorials*, Vol. 15, No. 3, pp. 996–1019, March 2013.

54. Gong, Z. and M. Haenggi, "Interference and Outage in Mobile Random Networks: Expectation, Distribution, and Correlation", *IEEE Transactions on Mobile Computing*, Vol. 13, No. 2, pp. 337–349, February 2014.

55. Bettstetter, C., G. Resta and P. Santi, "The node distribution of the random waypoint mobility model for wireless ad hoc networks", *IEEE Transactions on Mobile Computing*, Vol. 2, No. 3, pp. 257–269, July 2003.

APPENDIX A: PROOF OF THE THEOREMS

A.1. Proof of Equation (3.7)

If SINR of a user goes below the reuse threshold T_{FR}, user is allocated a new subband from reserved subbands for the edge users as a result of the reuse strategy. User y with $SINR < T_{FR}$ is assigned a new FFR subband δ_y, where $\delta \in 1, ..., \Delta$ with uniform probability $\frac{1}{\Delta}$. This results in a new fading power $\hat{g}$ and out-of-cell interference $\hat{I}$, which are different than initial g_y and I_r, respectively. Assuming $\hat{g}$ and g are i.i.d. exponentially distributed with mean μ, the CCDF of the edge user $F_{FFR}(T)$ is calculated by

$$\begin{aligned}
F_{FFR}(T) &= \mathbb{P}\left(\frac{P\hat{g}r^{-\alpha}}{\sigma^2 + P\hat{I}_r} > T \middle| \frac{Pgr^{-\alpha}}{\sigma^2 + PI_r} < T_{FR}\right) \\
&= \frac{\mathbb{P}\left(\frac{P\hat{g}r^{-\alpha}}{\sigma^2+P\hat{I}_r} > T, \frac{Pgr^{-\alpha}}{\sigma^2+PI_r} < T_{FR}\right)}{\mathbb{P}\left(\frac{Pgr^{-\alpha}}{\sigma^2+PI_r} < T_{FR}\right)} \\
&= \frac{\mathbb{E}\left[e^{-\mu\frac{T}{P}r^{\alpha}(\sigma^2+P\hat{I}_r)}\left(1 - e^{-\mu\frac{T_{FR}}{P}r^{\alpha}(\sigma^2+PI_r)}\right)\right]}{\mathbb{E}\left[1 - e^{-\mu\frac{T_{FR}}{P}r^{\alpha}(\sigma^2+PI_r)}\right]} \\
&= \frac{p_c(T,\lambda,\alpha,\Delta) - \mathbb{E}\left[e^{-\mu r^{\alpha}\frac{\sigma^2}{P}(T+T_{FR})}e^{-\mu r^{\alpha}(T\hat{I}_r+T_{FR}I_r)}\right]}{1 - p_c(T_{FR},\lambda,\alpha,1)}.
\end{aligned} \tag{A.1}$$

The expectation of $e^{-\mu r^{\alpha}(T\hat{I}_r+T_{FR}I_r)}$ gives the joint Laplace transform of $\hat{I}_r$ and I_r evaluated at $(\mu r^{\alpha}T, \mu r^{\alpha}T_{FR})$ when we condition on r. Letting $(s_1, s_2) = (\mu r^{\alpha}T, \mu r^{\alpha}T_{FR})$, the joint Laplace transform can be found as

$$\begin{aligned}\mathcal{L}(s_1, s_2) &= \mathbb{E}\left[exp\left(-s_1\hat{I}_r - s_2 I_r\right)\right] \\ &= \mathbb{E}\left[exp\left(-s_1\sum_{z\in Z}\hat{g}_z R_z^{-\alpha}\mathbf{1}(\delta_z = \delta_y) - s_2\sum_{z\in Z} g_z R_z^{-\alpha}\right)\right] \\ &= \mathbb{E}\left[\prod_{z\in Z} e^{s_2 g_z R_z^{-\alpha}}(1 - \mathbb{E}\left[\mathbf{1}(\delta_z = \delta_y)\right](1 - e^{s_1\hat{g}_z R_z^{-\alpha}}))\right].\end{aligned}$$

For the case in which the interference is also exponentially distributed, i.e. $\hat{g}_z$ and g_z are exponential with mean μ, joint Laplace transform becomes

$$\mathcal{L}(s_1, s_2) = \mathbb{E}\left[\prod_{z\in Z}\frac{\mu}{\mu + s_2 R_z^{-\alpha}}\left(1 - \frac{1}{\Delta}\left(1 - \frac{\mu}{\mu + s_1 R_z^{-\alpha}}\right)\right)\right]. \tag{A.2}$$

By using the probability generating functional (PGFL) of the PPP, joint Laplace functional is calculated by

$$\mathcal{L}(s_1, s_2) = exp\left(-2\pi\lambda\int_r^\infty\left[1 - \frac{\mu}{\mu + s_2 x^{-\alpha}}\left(1 - \frac{1}{\Delta}\left(1 - \frac{\mu}{\mu + s_1 x^{-\alpha}}\right)\right)\right]xdx\right).$$

By inserting s_1 and s_2 values into the equation, we obtain

$$\mathcal{L}(\mu r^{\alpha}T, \mu r^{\alpha}T_{FR}) = exp\left(-2\pi\lambda r^2 \int_1^{\infty}\left[1 - \frac{1}{1+T_{FR}x^{-\alpha}}\times \right.\right.$$
$$\left.\left.\left(1 - \frac{1}{\Delta}\left(1 - \frac{1}{1+Tx^{-\alpha}}\right)\right)\right]xdx\right). \quad \text{(A.3)}$$

If we decondition on r and insert the joint Laplace transform into the expectation of $e^{-\mu r^{\alpha}(T\hat{I}_r + T_{FR}I_r)}$, we can find the expectation to be

$$\mathbb{E}\left[e^{-\mu r^{\alpha}\frac{\sigma^2}{P}(T+T_{FR})}e^{-\mu r^{\alpha}(T\hat{I}_r + T_{FR}I_r)}\right] = \pi\lambda\int_0^{\infty} e^{-\pi\lambda v(1+2\xi(T,T_{FR},\alpha,\Delta))-\mu(T+T_{FR})\frac{\sigma^2}{P}v^{\alpha/2}}dv \quad \text{(A.4)}$$

where

$$\xi(T, T_{FR}, \alpha, \Delta) = \int_1^{\infty}\left[1 - \frac{1}{1+T_{FR}x^{-\alpha}}\left(1 - \frac{1}{\Delta}\left(1 - \frac{1}{1+Tx^{-\alpha}}\right)\right)\right]xdx. \quad \text{(A.5)}$$

Inserting the equation (A.4) into equation (A.1) gives the coverage probability of an edge user under strict FFR scheme.

A.2. Proof of Equation (4.6)

When $\alpha = 4$, $\xi(T, T_{FR}, \alpha, \Delta)$ turns into a closed form trigonometric equation instead of a numerically evaluated integral.

$$
\begin{aligned}
\xi(T, T_{FR}, 4, \Delta) &= \int_1^\infty \left[1 - \frac{1}{1 + T_{FR}x^{-4}}\left(1 - \frac{1}{\Delta}\left(1 - \frac{1}{1 + Tx^{-4}}\right)\right)\right] x dx \\
&= \int_1^\infty \frac{x}{\frac{x^4}{T_{FR}} + 1} dx + \int_1^\infty \frac{Tx^5}{\Delta(x^4 + T_{FR})(x^4 + T)} dx \\
&= \int_1^\infty \frac{x}{\frac{x^4}{T_{FR}} + 1} dx + \int_1^\infty \frac{Tx^5}{\Delta(x^4 + T_{FR})(x^4 + T)} dx \\
&= \int_1^\infty \frac{x}{\frac{x^4}{T_{FR}} + 1} dx + \int_1^\infty \frac{1}{\Delta}\left(\frac{\frac{-T^2 x}{T_{FR} - T}}{x^4 + T} + \frac{\frac{T_{FR}Tx}{T_{FR} - T}}{x^4 + T_{FR}}\right) dx \\
&= \int_1^\infty \frac{x}{(\frac{x^2}{\sqrt{T_{FR}}})^2 + 1} dx + \frac{1}{\Delta(T_{FR} - T)} \int_1^\infty \left(\frac{T_{FR}Tx}{x^4 + T} - \frac{T^2 x}{x^4 + T_{FR}}\right) dx \\
&= \int_1^\infty \frac{x}{(\frac{x^2}{\sqrt{T_{FR}}})^2 + 1} dx + \frac{1}{\Delta(T_{FR} - T)} \left(\int_{\frac{1}{\sqrt{T_{FR}}}}^\infty \frac{Tx}{(\frac{x^2}{\sqrt{T_{FR}}})^2 + 1} dx - \int_{\frac{1}{\sqrt{T}}}^\infty \frac{Tx}{(\frac{x^2}{\sqrt{T_{FR}}})^2 + 1} dx\right) \\
&= \int_{\frac{1}{\sqrt{T_{FR}}}}^\infty \frac{\sqrt{T_{FR}}}{2} \frac{du}{u^2 + 1} + \frac{1}{\Delta(T_{FR} - T)} \left(\int_{\frac{1}{\sqrt{T_{FR}}}}^\infty \frac{T\sqrt{T_{FR}}}{2} \frac{du}{u^2 + 1} - \int_{\frac{1}{\sqrt{T}}}^\infty \frac{T\sqrt{T}}{2} \frac{du_2}{u_2^2 + 1}\right) \\
&= \frac{\sqrt{T_{FR}}}{2} \arctan u \Big|_{\frac{1}{\sqrt{T_{FR}}}}^\infty + \frac{1}{\Delta(T_{FR} - T)} \left(\frac{T\sqrt{T_{FR}}}{2} \arctan u \Big|_{\frac{1}{\sqrt{T_{FR}}}}^\infty - \frac{T\sqrt{T}}{2} \arctan u \Big|_{\frac{1}{\sqrt{T}}}^\infty\right) \\
&= \frac{\sqrt{T_{FR}}}{2} \arctan \sqrt{T_{FR}} + \frac{1}{\Delta(T_{FR} - T)} \left(\frac{T\sqrt{T_{FR}}}{2} \arctan \sqrt{T_{FR}} - \frac{T\sqrt{T}}{2} \arctan \sqrt{T}\right) \\
&= \frac{1}{2}\rho(T_{FR}, 4) + \frac{T}{\Delta(T_{FR} - T)} \left(\frac{1}{2}\rho(T_{FR}, 4) - \frac{1}{2}\rho(T, 4)\right) \\
&= \frac{T\rho(T, 4) - \rho(T_{FR}, 4)(T_{FR}\Delta - T(\Delta - 1))}{2\Delta(T - T_{FR})}
\end{aligned}
\tag{A.6}
$$

where

$$
\rho(T, 4) = \sqrt{T} arctan(\sqrt{T}) \tag{A.7}
$$

A.3. Proof of Equation (3.13)

User y with $SINR < T_{FR}$ is given a different SFR sub-band δ_y, where $\delta \in 1, ..., \Delta$ with a transmit power of βP. This results in a new fading power $\hat{g}$ and out-of-cell interference $\hat{I}$, which are different than initial g_y and I_r, respectively. Assuming $\hat{g}$ and g are i.i.d. exponentially distributed with mean μ, the CCDF of the edge user $F_{SFR}(T)$ is calculated by

$$\begin{aligned}
F_{SFR}(T) &= \mathbb{P}\left(\frac{\beta P \hat{g} r^{-\alpha}}{\sigma^2 + \eta P \hat{I}_r} > T \middle| \frac{P g r^{-\alpha}}{\sigma^2 + \eta P I_r} < T_{FR}\right) \\
&= \frac{\mathbb{P}\left(\frac{\beta P \hat{g} r^{-\alpha}}{\sigma^2+\eta P \hat{I}_r} > T, \frac{P g r^{-\alpha}}{\sigma^2+\eta P I_r} < T_{FR}\right)}{\mathbb{P}\left(\frac{P g r^{-\alpha}}{\sigma^2+\eta P I_r} < T_{FR}\right)} \\
&= \frac{\mathbb{E}\left[e^{-\mu \frac{T}{\beta P} r^{\alpha}(\sigma^2+\eta P \hat{I}_r)}\left(1 - e^{-\mu \frac{T_{FR}}{P} r^{\alpha}(\sigma^2+\eta P I_r)}\right)\right]}{\mathbb{E}\left[1 - e^{-\mu \frac{T_{FR}}{P} r^{\alpha}(\sigma^2+\eta P I_r)}\right]} \\
&= \frac{p_c(\eta \frac{T}{\beta}, \lambda, \alpha, \Delta) - \mathbb{E}\left[e^{-\mu r^{\alpha} \frac{\sigma^2}{P}(\frac{T}{\beta}+T_{FR})} e^{-\mu r^{\alpha} \eta (\frac{T}{\beta}\hat{I}_r + T_{FR} I_r)}\right]}{1 - p_c(\eta T_{FR}, \lambda, \alpha, 1)}.
\end{aligned} \tag{A.8}$$

If we condition on r in the second term, we can notice that the expectation of $e^{-\mu r^{\alpha} \eta (\frac{T}{\beta}\hat{I}_r + T_{FR} I_r)}$ results in the joint Laplace transform of $\hat{I}_r$ and I_r evaluated at $(\mu r^{\alpha} \eta \frac{T}{\beta}, \mu r^{\alpha} \eta T_{FR})$. In the strict FFR case, $\hat{I}_r$ and I is caused by BSs that are only associated with the user's sub-band δ. However, in SFR case, interference comes from all the BSs and this is equivalent of $\Delta = 1$. Thus the joint Laplace transform is found as

$$\mathcal{L}(s_1, s_2) = \mathbb{E}\left[\prod_{z \in Z} \frac{\mu}{\mu + s_2 R_z^{-\alpha}} \frac{\mu}{\mu + s_1 R_z^{-\alpha}}\right]. \tag{A.9}$$

By using the probability generating functional (PGFL) of the PPP, Laplace functional is calculated as

$$\mathcal{L}(s_1, s_2) = exp\left(-2\pi\lambda \int_r^{\infty} \left[1 - \frac{\mu}{\mu + s_2 x^{-\alpha}} \frac{\mu}{\mu + s_1 x^{-\alpha}}\right] x dx\right). \tag{A.10}$$

By inserting s_1 and s_2, we obtain

$$\mathcal{L}(\mu r^{\alpha}\eta\frac{T}{\beta}, \mu r^{\alpha}\eta T_{FR}) = exp\left(-2\pi\lambda r^2 \int_1^{\infty} \left[1 - \frac{1}{1 + \eta T_{FR} x^{-\alpha}} \frac{1}{1 + \eta\frac{T}{\beta} x^{-\alpha}}\right] x dx\right). \tag{A.11}$$

Deconditioning on r gives

$$\mathbb{E}\left[e^{-\mu r^{\alpha}\frac{\sigma^2}{P}(\eta\frac{T}{\beta}+\eta T_{FR})} e^{-\mu r^{\alpha}(\eta\frac{T}{\beta}\hat{I}_r + \eta T_{FR} I_r)}\right] = \pi\lambda \int_0^{\infty} e^{-\pi\lambda v(1+2\zeta(T,T_{FR},\alpha,1,\eta,\beta))} \times e^{-\mu(\eta\frac{T}{\beta}+\eta T_{FR})\frac{\sigma^2}{P}\upsilon^{\alpha/2}} d\upsilon, \tag{A.12}$$

where

$$\zeta(T, T_{FR}, \alpha, 1, \eta, \beta) = \int_1^{\infty} \left[1 - \frac{1}{1 + \eta T_{FR} x^{-\alpha}} \frac{1}{1 + \eta\frac{T}{\beta} x^{-\alpha}}\right] x dx. \tag{A.13}$$

Inserting the equation (A.12) into equation (3.13) gives the coverage probability of an edge user under SFR scheme.

A.4. Proof of Equation (3.15)

When $\alpha = 4$, $\zeta(T, T_{FR}, 4, \eta, \beta)$ turns into a closed form trigonometric equation instead of a numerically evaluated integral.

$$\begin{aligned}
\zeta(T, T_{FR}, 4,\eta, \beta) &= \int_1^\infty \left[1 - \frac{1}{1+\eta T_{FR} x^{-\alpha}} \frac{1}{1+\eta\frac{T}{\beta} x^{-\alpha}}\right] x dx \\
&= \int_1^\infty \left[1 - \frac{x^4\frac{\eta}{\beta}T^4 + x^4\eta T_{FR}^4 + \frac{\eta^2}{\beta}T^4 T_{FR}^4}{(x^4+\eta T_{FR})(x^4+\frac{\eta}{\beta}T)}\right] x dx \\
&= \int_1^\infty \left[1 - \frac{x^4\frac{\eta}{\beta}T^4 + x^4\eta T_{FR}^4 + \frac{\eta^2}{\beta}T^4 T_{FR}^4}{(x^4+\eta T_{FR})(x^4+\frac{\eta}{\beta}T)}\right] x dx \\
&= \int_1^\infty \frac{\frac{\frac{\eta}{\beta}T^2}{T-\beta T_{FR}}}{x^4+\frac{\eta}{\beta}T} x dx + \int_1^\infty \frac{\frac{\eta\beta T_{FR}^2}{T-\beta T_{FR}}}{x^4+\eta T_{FR}} x dx \\
&= \int_1^\infty \frac{\frac{T}{T-\beta T_{FR}}}{\frac{x^4}{\frac{\eta}{\beta}T}+1} x dx + \int_1^\infty \frac{\frac{\beta T_{FR}}{T-\beta T_{FR}}}{\frac{x^4}{\eta T_{FR}}+1} x dx \\
&= \int_{1/\sqrt{\frac{\eta}{\beta}T}}^\infty \frac{\sqrt{\frac{\eta}{\beta}T}}{2} \frac{T}{T-\beta T_{FR}} \frac{du}{u^2+1} + \int_{1/\sqrt{\eta T_{FR}}}^\infty \frac{\sqrt{\eta T_{FR}}}{2} \frac{\beta T_{FR}}{T-\beta T_{FR}} \frac{du_2}{u_2^2+1} \\
&= \frac{\sqrt{\frac{\eta}{\beta}T}}{2} \frac{T}{T-\beta T_{FR}} arctan(\sqrt{\frac{\eta}{\beta}T}) + \frac{\sqrt{\eta T_{FR}}}{2} \frac{T}{T-\beta T_{FR}} arctan(\sqrt{\eta T_{FR}}) \\
&= \frac{1}{2(T-\beta T_{FR})} \left(T\rho(\frac{\eta}{\beta}T, 4) - \beta T_{FR}\rho(\eta T_{FR}, 4)\right)
\end{aligned} \tag{A.14}$$

where $\rho(T, 4)$ is given in (3.10).

A.5. Proof of Equation (4.2)

Under strict FFR technique, a mobile user first determines its SINR to the nearest BS of the k^{th} tier and checks if it is less than the tier's FFR threshold T_k. If so, user is classified as an edge user and the BS transmits its downlink on the reserved FFR band, randomly picked from Δ_k subbands available with uniform probability $\frac{1}{\Delta}$. Otherwise, we classify the mobile user as an interior user. Strict FFR edge user experiences new fading power $\hat{g_k}$ and out-of-cell interference $P_k\hat{I_k}$, instead of g_k and $\sum_{j\neq k}^{K} P_j I_j$, which are different than initial g_k and $\sum_{j\neq k}^{K} P_j I_j$. Assuming $\hat{g}$ and g_k are i.i.d. exponentially distributed with mean μ, and following the similar approaches in the previous section, the CCDF of the edge user $F_{FFR,cl}(T)$ is calculated by

$$
\begin{aligned}
F_{FFR,cl}(T) &= \mathbb{P}\left(\frac{P_k\hat{g_k}r_k^{-\alpha}}{\sigma^2+P_k\hat{I_k}} > T \middle| \frac{P_k g_k r_k^{-\alpha}}{\sigma^2+\sum_{j\neq k}^{K} P_j I_j} < T_k\right) \\
&= \frac{\mathbb{P}\left(\frac{P_k\hat{g_k}r_k^{-\alpha}}{\sigma^2+P_k\hat{I_k}} > T, \frac{P_k g_k r_k^{-\alpha}}{\sigma^2+\sum_{j\neq k}^{K} P_j I_j} < T_k\right)}{\mathbb{P}\left(\frac{P_k g_k r_k^{-\alpha}}{\sigma^2+\sum_{j\neq k}^{K} P_j I_j} < T_k\right)} \\
&= \frac{\mathbb{E}\left[e^{-\mu\frac{T}{P_k}r_k^{\alpha}(\sigma^2+P_k\hat{I_k})}\left(1-e^{-\mu\frac{T_k}{P_k}r_k^{\alpha}(\sigma^2+P_kI_k+\sum_{j\neq k}^{K}P_jI_j)}\right)\right]}{\mathbb{E}\left[1-e^{-\mu\frac{T_k}{P_k}r_k^{\alpha}(\sigma^2+P_kI_k+\sum_{j\neq k}^{K}P_jI_j)}\right]}.
\end{aligned}
$$

After factoring out the terms related with noise power σ^2, if we condition on Rayleigh distributed r_k in the second term, we observe that expectation of remaining terms is the joint Laplace transform of $\hat{I_k}$ and $I_1, I_2, ...I_K$ which is found as

$$\mathcal{L}(\hat{s_k}, s_1, .., s_K) = \mathbb{E}\left[exp\left(-\hat{s_k}\hat{I_k} - s_k I_k - \sum_{j\neq k}^{K} s_j I_j\right)\right]$$

$$= \mathbb{E}\left[exp\left(-\hat{s_k}\sum_{z\in Z_k}\hat{g_z}R_z^{-\alpha}\mathbf{1}(\delta_z = \delta_y) - s_k g_z R_z^{-\alpha}\right) \times exp\left(-\sum_{j\neq k}^{K}(s_j \sum_{z\in Z_j} g_j R_z^{-\alpha})\right)\right]$$

$$= \mathbb{E}\left[\prod_{z\in Z}(1 - \mathbb{E}\left[\mathbf{1}(\delta_z = \delta_y)\right](1 - e^{-\hat{s_k}\hat{g_z}R_z^{-\alpha}})e^{-s_k g_z R_z^{-\alpha}}\right] \times \prod_{j\neq k}^{K}\mathbb{E}\left[\prod_{z\in Z_j} e^{-s_j g_z R_z^{-\alpha}}\right].$$

Assuming interference is also exponentially distributed, i.e. $\hat{g_z}$ and g_z are also exponential with mean μ ,

$$\mathcal{L}(\hat{s_k}, s_1, .., s_K) = \mathbb{E}\left[\prod_{z\in Z_k}\left(1 - \frac{1}{\Delta_k}\left(1 - \frac{\mu}{\mu + \hat{s_k}R_z^{-\alpha}}\right)\right)\frac{\mu}{\mu + s_k R_z^{-\alpha}}\right] \times \prod_{j\neq k}^{K}\mathbb{E}\left[\prod_{z\in Z_j}\frac{\mu}{\mu + s_j R_z^{-\alpha}}\right]$$

By using the probability generating functional (PGFL) of the PPP, Laplace functional is calculated by

$$\mathcal{L}(\hat{s_k}, s_1, .., s_K) = exp\left(-2\pi\lambda_1\int_{r_1}^{\infty}\left[1 - \frac{\mu}{\mu + s_k x^{-\alpha}}\left(1 - \frac{1}{\Delta}\left(1 - \frac{\mu}{\mu + \hat{s_k}x^{-\alpha}}\right)\right)\right]xdx\right) \times \prod_{j\neq k}^{K} exp\left(-2\pi\lambda_j(\frac{s_j}{\mu})^{2/\alpha}\frac{\pi csc(\frac{2\pi}{\alpha})}{\alpha}\right). \tag{A.15}$$

Inserting evaluated points into the integration variables s and deconditioning on r_k result in

$$2\pi r_k\lambda_k\int_0^{\infty} e^{-\pi\lambda_k r_k^2(1+2\xi(T,T_k,\alpha,\Delta_k))}e^{-2\pi\lambda_k r_k^2(\sum_{j\neq k}^{K}\kappa_{j,k}\psi(\gamma_{j,k}T_k,\alpha))}e^{-\mu(T+T_k)\frac{\sigma^2}{P_k}r_k^{\alpha}}dr_k \tag{A.16}$$

where

$$\xi(T,T_k,\alpha,\Delta_k)=\int_{r_k}^{\infty}\left[1-\frac{1}{1+T_k r_k^{\alpha}x^{-\alpha}}\left(1-\frac{1}{\Delta_k}\left(1-\frac{1}{1+Tr_k^{\alpha}x^{-\alpha}}\right)\right)\right]xdx \quad \text{(A.17)}$$

and

$$\psi(z,\alpha)=\frac{\pi z^{2/\alpha}}{\alpha}csc(\frac{2\pi}{\alpha}),\gamma_{j,k}=\frac{P_j}{P_k},\kappa_{j,k}=\frac{\lambda_j}{\lambda_k}.$$

By using similar techniques, denominator becomes

$$1-\mathbb{E}\left[e^{-\mu\frac{T_k}{P_k}r_k^{\alpha}(\sigma^2+P_kI_k+\sum_{j\neq k}^{K}P_jI_j)}\right]=1-\mathbb{E}\left[e^{-\mu\frac{T_k}{P_k}r_k^{\alpha}(\sigma^2+P_kI_k)}\right]\times\prod_{j\neq k}^{K}\mathbb{E}e^{-\mu\frac{T_k}{P_k}r_k^{\alpha}P_jI_j}$$
$$=1-2\pi r_k\lambda_k\int_0^{\infty}e^{-\pi\lambda_k r_k^2(1+2\rho(T_k,\alpha))}e^{-2\pi\lambda_k r_k^2(\sum_{j\neq k}^{K}\kappa_{j,k}\psi(\gamma_{j,k}T_k,\alpha))}e^{-\mu(T+T_k)\frac{\sigma^2}{P_k}r_k^{\alpha}}dr_k$$

and after substituting $r_k^2=\upsilon$ the first term of the numerator which represents the SINR on the newly allocated subband becomes

$$\pi\lambda_k\int_0^{\infty}e^{-\pi\lambda_k\upsilon(1+\frac{\rho(T_k,\alpha)}{\Delta_k})}e^{-\mu(T+T_k)\frac{\sigma^2}{P_k}\upsilon^{\alpha/2}}d\upsilon.$$

Thus, overall equation becomes

$$F_{FFR,cl}(k,T)$$
$$=\frac{\pi\lambda_k\int_0^{\infty}e^{-\pi\lambda_k\upsilon(1+\frac{\rho(T_k,\alpha)}{\Delta_k})}e^{-\mu(T+T_k)\frac{\sigma^2}{P_k}\upsilon^{\alpha/2}}d\upsilon}{1-\pi\lambda_k\int_0^{\infty}e^{-\pi\lambda_k\upsilon(1+\rho(T_k,\alpha))}e^{-2\pi\lambda_k\upsilon(\sum_{j\neq k}^{K}\kappa_{j,k}\psi(\gamma_{j,k}T_k,\alpha))}e^{-\mu(T+T_k)\frac{\sigma^2}{P_k}\upsilon^{\alpha/2}}d\upsilon}-$$
$$\frac{\pi\lambda_k\upsilon\int_0^{\infty}e^{-\pi\lambda_k\upsilon(1+2\xi(T,T_k,\alpha,\Delta_k))}e^{-2\pi\lambda_k\upsilon(\sum_{j\neq k}^{K}\kappa_{j,k}\psi(\gamma_{j,k}T_k,\alpha))}e^{-\mu(T+T_k)\frac{\sigma^2}{P_k}\upsilon^{\alpha/2}}d\upsilon}{1-\pi\lambda_k\int_0^{\infty}e^{-\pi\lambda_k\upsilon(1+\rho(T_k,\alpha))}e^{-2\pi\lambda_k\upsilon(\sum_{j\neq k}^{K}\kappa_{j,k}\psi(\gamma_{j,k}T_k,\alpha))}e^{-\mu(T+T_k)\frac{\sigma^2}{P_k}\upsilon^{\alpha/2}}d\upsilon}. \quad \text{(A.18)}$$

A.6. Proof of Section 4.2.1

A cellular user is assigned a different FFR subband δ_y, with $1/\Delta$ uniform probability, if $SIR_1 < T_1$ and $SIR_2 < T_2$, where T_1 is the open access threshold for the first tier BSs and T_2 is the open access threshold for the second tier APs. The new SIR after this assignment is calculated by $\hat{SIR} = \frac{P_1 \hat{g_1} r_1^{-\alpha}}{P_1 \hat{I_1}}$ for the first tier SIR and the coverage probability of the cell-edge user under open access method can be calculated by

$$\begin{aligned} F_{FFR,open,edge}(T) &= \mathbb{P}\left(\hat{SIR} > T | SIR_1 < T_1, SIR_2 < T_2\right) \\ &= \mathbb{P}\left(\frac{P_1 \hat{g_1} r_1^{-\alpha}}{P_1 \hat{I_1}} > T \middle| SIR_1 < T_1, SIR_2 < T_2\right) \\ &= \frac{\mathbb{P}\left(\frac{P_1 \hat{g_1} r_1^{-\alpha}}{P_1 \hat{I_1}} > T, \frac{P_1 g_1 r_1^{-\alpha}}{P_1 I_1 + P_2 I_2 + P_2 g_2 r_2^{-\alpha}} < T_1, \frac{P_2 g_2 r_2^{-\alpha}}{P_1 I_1 + P_2 I_2 + P_1 g_1 r_1^{-\alpha}} < T_2\right)}{\mathbb{P}\left(\frac{P_1 g_1 r_1^{-\alpha}}{P_1 I_1 + P_2 I_2 + P_2 g_2 r_2^{-\alpha}} < T_1, \frac{P_2 g_2 r_2^{-\alpha}}{P_1 I_1 + P_2 I_2 + P_1 g_1 r_1^{-\alpha}} < T_2\right)}. \end{aligned}$$

If we focus on the denominator first, conditioning on g_2 gives

$$\mathbb{P}\left[\frac{r_1^\alpha}{P_1}\left(\frac{P_2}{T_2} g_2 r_2^{-\alpha} - (P_1 I_1 + P_2 I_2)\right) < g_1 < T_1 \frac{r_1^\alpha}{P_1}(P_1 I_1 + P_2 I_2 + P_2 g_2 r_2^{-\alpha}) | g_2\right] \mathbb{P}(g_2). \tag{A.19}$$

Since g_1 and g_2 are i.i.d. exponentially distributed with mean μ and defining $\bar{I} = P_1 I_1 + P_2 I_2$ gives

$$\mathbb{E}_{g_2}\left[\int_{\frac{r_1^\alpha}{P_1}\left(\frac{P_2}{T_2} g_2 r_2^{-\alpha} - \bar{I}\right)^+}^{T_1 \frac{r_1^\alpha}{P_1}(\bar{I} + P_2 g_2 r_2^{-\alpha})} \mu e^{-\mu x} dx\right] = \mathbb{E}_{g_2}\left[e^{-\mu \frac{r_1^\alpha}{P_1}\left(\frac{P_2}{T_2} g_2 r_2^{-\alpha} - \bar{I}\right)^+} - e^{-\mu T_1 \frac{r_1^\alpha}{P_1}(\bar{I} + P_2 g_2 r_2^{-\alpha})}\right] \tag{A.20}$$

where $(x)^+ = \begin{cases} x : x > 0 \\ 0 : x \leq 0 \end{cases}$. Evaluating the expectations results in

$$1 - \epsilon_1 e^{-\mu \frac{T_1}{P_1} r_1^\alpha \bar{I}} + (\epsilon_2 - 1) e^{-\mu \frac{T_2}{P_2} r_2^\alpha \bar{I}}, \tag{A.21}$$

where

$$\epsilon_1 = \frac{1}{T_1\gamma\frac{r_1^\alpha}{r_2^\alpha}+1}$$
$$\epsilon_2 = \frac{1}{\frac{\gamma}{T_2}\frac{r_1^\alpha}{r_2^\alpha}+1} \; and \; \gamma = \frac{P_2}{P_1}.$$

Expectation of (A.21) with respect to I_1 and I_2 results in the joint Laplace transform of I_1 and I_2, which can be calculated as follows.

$$\begin{aligned}
\mathcal{L}(s_1,s_2) &= \mathbb{E}_{I_1,I_2}\left[1-\epsilon_1 e^{-\mu\frac{T_1}{P_1}r_1^\alpha(P_1I_1+P_2I_2)}+(\epsilon_2-1)e^{-\mu\frac{T_2}{P_2}r_2^\alpha(P_1I_1+P_2I_2)}\right] \\
&= \mathbb{E}_{I_1,I_2}\Big[1-\epsilon_1 e^{-\mu T_1 r_1^\alpha\sum_{z\in Z_1}g_1R_z^{-\alpha}}e^{-\mu T_1\gamma r_1^\alpha\sum_{z\in Z_2}g_2R_z^{-\alpha}}+ \\
&\quad (\epsilon_2-1)e^{-\mu\frac{T_2}{\gamma}r_2^\alpha\sum_{z\in Z_1}g_1R_z^{-\alpha}}e^{-\mu T_2 r_2^\alpha\sum_{z\in Z_2}g_2R_z^{-\alpha}}\Big] \\
&= 1-\epsilon_1\mathbb{E}_{I_1,I_2}\left[\prod_{z\in Z_1}e^{-s_1g_1R_z^{-\alpha}}\right]\mathbb{E}_{I_1,I_2}\left[\prod_{z\in Z_2}e^{-s_2g_2R_z^{-\alpha}}\right]+ \\
&\quad (\epsilon_2-1)\mathbb{E}_{I_1,I_2}\left[\prod_{z\in Z_1}e^{-s_1'g_1R_z^{-\alpha}}\right]\mathbb{E}_{I_1,I_2}\left[\prod_{z\in Z_2}e^{-s_2'g_2R_z^{-\alpha}}\right].
\end{aligned}$$

By considering that g_1 and g_2 are also exponential with mean μ, joint Laplace transform becomes

$$\begin{aligned}
\mathcal{L}(s_1,s_2) &= 1-\epsilon_1\mathbb{E}_{I_1,I_2}\left[\prod_{z\in Z_1}\frac{\mu}{\mu+s_1R_z^{-\alpha}}\right]\mathbb{E}_{I_1,I_2}\left[\prod_{z\in Z_2}\frac{\mu}{\mu+s_2R_z^{-\alpha}}\right]+ \\
&\quad (\epsilon_2-1)\mathbb{E}_{I_1,I_2}\left[\prod_{z\in Z_1}\frac{\mu}{\mu+s_1'R_z^{-\alpha}}\right]\mathbb{E}_{I_1,I_2}\left[\prod_{z\in Z_2}\frac{\mu}{\mu+s_2'R_z^{-\alpha}}\right].
\end{aligned}$$

By using the probability generating functional (PGFL) of the PPP, $\mathcal{L}(s_1,s_2)$ turns into

$$\begin{aligned}
\mathcal{L}(s_1,s_2) &= 1-\epsilon_1 e^{-2\pi\lambda_1\int_{r_1}^\infty\left(1-\frac{\mu}{\mu+s_1x^{-\alpha}}\right)xdx}\times e^{-2\pi\lambda_2(\frac{s_2}{\mu})^{2/\alpha}\frac{\pi}{\alpha}csc(\frac{2\pi}{\alpha})}+ \\
&\quad (\epsilon_2-1)e^{-2\pi\lambda_1\int_{r_1}^\infty\left(1-\frac{\mu}{\mu+s_1'x^{-\alpha}}\right)xdx}\times e^{-2\pi\lambda_2(\frac{s_2'}{\mu})^{2/\alpha}\frac{\pi}{\alpha}csc(\frac{2\pi}{\alpha})}.
\end{aligned}$$

Inserting evaluated points into the integration variable s gives

$$\mathcal{L}(\mu r_1^{\alpha} T_1, \mu r_2^{\alpha} T_2) = 1 - \epsilon_1 e^{-2\pi\lambda_1 \int_{r_1}^{\infty} \left(1 - \frac{1}{1+T_1 r_1^{\alpha} x^{-\alpha}}\right) x dx} \times e^{-2\pi\lambda_2 (\gamma T_1)^{2/\alpha} r_1^2 \frac{\pi}{\alpha} csc(\frac{2\pi}{\alpha})} + (\epsilon_2 - 1) e^{-2\pi\lambda_1 \int_{r_2}^{\infty} \left(1 - \frac{1}{1+T_2 r_2^{\alpha} x^{-\alpha}}\right) x dx} \times e^{-2\pi\lambda_1 (\frac{T_2}{\gamma})^{2/\alpha} r_2^2 \frac{\pi}{\alpha} csc(\frac{2\pi}{\alpha})}.$$

If we deconditon on r_1 and r_2, denominator results in

$$f_d(r_1, r_2) = 1 - \epsilon_1 \int_0^{\infty} 2\pi\lambda_1 r_1 e^{-2\pi\lambda_1 r_1^2 (\rho_1(T_1,\alpha) + 1 + \kappa\psi(\gamma T_1, \alpha))} dr_1 + (\epsilon_2 - 1) \int_0^{\infty} 2\pi\lambda_2 r_2 e^{-2\pi\lambda_2 r_2^2 (\rho_2(T_2,\alpha) + 1 + \frac{1}{\kappa}\psi(\frac{T_2}{\gamma}, \alpha))} dr_2, \tag{A.22}$$

where

$$\rho_1(T_1, \alpha) = \int_{r_1}^{\infty} \left(1 - \frac{1}{1 + T_1 r_1^{\alpha} x^{-\alpha}}\right) x dx$$
$$\rho_2(T_2, \alpha) = \int_{r_2}^{\infty} \left(1 - \frac{1}{1 + T_2 r_2^{\alpha} x^{-\alpha}}\right) x dx$$
$$\psi(z, \alpha) = \frac{\pi z^{2/\alpha}}{\alpha} csc(\frac{2\pi}{\alpha})$$
$$\gamma = \frac{P_2}{P_1}, \kappa = \frac{\lambda_2}{\lambda_1}.$$

Secondly, by focusing on the numerator, we can find numerator as follows.

$$
\begin{aligned}
&f_n(r_1,r_2)=\mathbb{E}_{\hat{I}_1,I_1,I_2}\Big[e^{-\mu\hat{I}_1 T r_1^{\alpha}}\left(1-\epsilon_1 e^{-\mu\frac{T_1}{P_1}r_1^{\alpha}(P_1I_1+P_2I_2)}+(\epsilon_2-1)e^{-\mu\frac{T_2}{P_2}r_2^{\alpha}(P_1I_1+P_2I_2)}\right)\Big]\\
&=p_c(T,\lambda_1,\alpha,\Delta)-\epsilon_1\mathbb{E}\left[e^{-\hat{s_1}\sum_{z\in Z_1}\hat{g_z}R_z^{-\alpha}\mathbf{1}(\delta_z=\delta_y)-s_1g_zR_z^{-\alpha}}e^{(-s_2\sum_{z\in Z_2}g_zR_z^{-\alpha})}\right]+\\
&(\epsilon_2-1)\mathbb{E}\left[e^{-\hat{s_1}\sum_{z\in Z_1}\hat{g_z}R_z^{-\alpha}\mathbf{1}(\delta_z=\delta_y)-s_1'g_zR_z^{-\alpha}}e^{(-s_2'\sum_{z\in Z_2}g_zR_z^{-\alpha})}\right]\\
&=p_c(T,\lambda_1,\alpha,\Delta)-\\
&\epsilon_1\mathbb{E}\left[\prod_{z\in Z}(1-\mathbb{E}\left[\mathbf{1}(\delta_z=\delta_y)\right](1-e^{-\hat{s_1}\hat{g_z}R_z^{-\alpha}})e^{-s_1g_zR_z^{-\alpha}}\right]\times\mathbb{E}\left[\prod_{z\in Z_2}e^{-s_2g_zR_z^{-\alpha}}\right]+\\
&(\epsilon_2-1)\mathbb{E}\left[\prod_{z\in Z}(1-\mathbb{E}\left[\mathbf{1}(\delta_z=\delta_y)\right](1-e^{-\hat{s_1}\hat{g_z}R_z^{-\alpha}})e^{-s_1'g_zR_z^{-\alpha}}\right]\times\mathbb{E}\left[\prod_{z\in Z_2}e^{-s_2'g_zR_z^{-\alpha}}\right]\\
&=p_c(T,\lambda_1,\alpha,\Delta)-\\
&\epsilon_1\mathbb{E}\left[\prod_{z\in Z_1}\left(1-\frac{1}{\Delta}\left(1-\frac{\mu}{\mu+\hat{s_1}R_z^{-\alpha}}\right)\right)\frac{\mu}{\mu+s_1R_z^{-\alpha}}\right]\times\mathbb{E}\left[\prod_{z\in Z_2}\frac{\mu}{\mu+s_2R_z^{-\alpha}}\right]+\\
&(\epsilon_2-1)\mathbb{E}\left[\prod_{z\in Z_1}\left(1-\frac{1}{\Delta}\left(1-\frac{\mu}{\mu+\hat{s_1'}R_z^{-\alpha}}\right)\right)\frac{\mu}{\mu+s_1'R_z^{-\alpha}}\right]\times\mathbb{E}\left[\prod_{z\in Z_2}\frac{\mu}{\mu+s_2'R_z^{-\alpha}}\right]\\
&=p_c(T,\lambda_1,\alpha,\Delta)-\\
&\epsilon_1\left(e^{-2\pi\lambda_1\int_{r_1}^{\infty}\left[1-\frac{1}{1+T_1r_1^{\alpha}x^{-\alpha}}\left(1-\frac{1}{\Delta}\left(1-\frac{1}{1+Tr_1^{\alpha}x^{-\alpha}}\right)\right)\right]xdx}e^{-2\pi\lambda_2(\gamma T_1)^{2/\alpha}r_1^2\frac{\pi}{\alpha}csc(\frac{2\pi}{\alpha})}\right)+\\
&(\epsilon_2-1)\left(e^{-2\pi\lambda_1\int_{r_1}^{\infty}\left[1-\frac{1}{1+\frac{T_2}{\alpha}r_2^{\alpha}x^{-\alpha}}\left(1-\frac{1}{\Delta}\left(1-\frac{1}{1+Tr_1^{\alpha}x^{-\alpha}}\right)\right)\right]xdx}e^{-2\pi\lambda_2(T_2/\gamma)^{2/\alpha}r_2^2\frac{\pi}{\alpha}csc(\frac{2\pi}{\alpha})}\right).
\end{aligned}
$$

Deconditioning on r_1 and r_2 gives

$$
\begin{aligned}
&f_n(r_1,r_2)=p_c(T,\lambda_1,\alpha,\Delta)-\epsilon_1\left(\int_0^{\infty}2\pi r_1\lambda_1e^{-\pi\lambda_1{r_1}^2(1+\xi_1(T,T_1,\alpha,\Delta))}e^{-2\pi\lambda_1{r_1}^2\kappa\psi(\gamma T_1,\alpha)}dr_1\right)\\
&+(\epsilon_2-1)\left(\int_0^{\infty}\int_0^{\infty}2\pi r_1\lambda_1 2\pi r_2\lambda_2e^{-\pi\lambda_1{r_1}^2(1+\xi_2(T,T_2/\gamma,\alpha,\Delta))}e^{-2\pi\lambda_2{r_2}^2(1+\frac{1}{\kappa}\psi(T_2/\gamma,\alpha))}dr_1dr_2\right)
\end{aligned}
\tag{A.23}
$$

where

$$\xi_1(T, T_1, \alpha, \Delta) = \int_{r_1}^{\infty} \left[1 - \frac{1}{1 + T_1 r_1^{\alpha} x^{-\alpha}} \left(1 - \frac{1}{\Delta}\left(1 - \frac{1}{1 + T r_1^{\alpha} x^{-\alpha}}\right)\right)\right] x dx \tag{A.24}$$

$$\xi_2(T, T_2/\gamma, \alpha, \Delta) = \int_{r_1}^{\infty} \left[1 - \frac{1}{1 + (T_2/\gamma) r_2^{\alpha} x^{-\alpha}} \left(1 - \frac{1}{\Delta}\left(1 - \frac{1}{1 + T r_1^{\alpha} x^{-\alpha}}\right)\right)\right] x dx \tag{A.25}$$

and

$$\psi(z, \alpha) = \frac{\pi z^{2/\alpha}}{\alpha} csc(\frac{2\pi}{\alpha}), \gamma = \frac{P_2}{P_1}, \kappa = \frac{\lambda_2}{\lambda_1}.$$

One can obtain the coverage probability of strict FFR scheme by inserting (A.22) and (A.23) into following formula

$$F_{FFR,open,edge}(k, T) = \frac{f_n(r_1, r_2)}{f_d(r_1, r_2)}.$$